



Emirates Mars Mission Characterization of Mars Atmosphere Dynamics and Processes

Hessa Almatroushi¹ · Hoor AlMazmi² · Noora AlMheiri¹ · Mariam AlShamsi¹ · Eman AlTunajji¹ · Khalid Badri¹ · Robert J. Lillis³ · Fatma Lootah¹ · Maryam Yousuf¹ · Sarah Amiri¹ · David A. Brain⁴ · Michael Chaffin⁴ · Justin Deighan⁴ · Christopher S. Edwards⁵ · Francois Forget⁶ · Michael D. Smith⁷ · Michael J. Wolff⁸ · Philip R. Christensen⁹ · Scott England¹⁰ · Matthew Fillingim³ · Gregory M. Holsclaw⁴ · Sonal Jain⁴ · Andrew R. Jones⁴ · Mikki Osterloo⁸ · Bruce M. Jakosky⁴ · Janet G. Luhmann³ · Roland M. B. Young¹¹

Received: 19 November 2020 / Accepted: 14 September 2021 / Published online: 7 December 2021
© The Author(s) 2021

Abstract

The Emirates Mars Mission (EMM) – Hope Probe – was developed to understand Mars atmospheric circulation, dynamics, and processes through characterization of the Mars atmosphere layers and its interconnections enabled by a unique high-altitude (19,970 km periapse and 42,650 km apoapse) low inclination orbit that will offer an unprecedented local and seasonal time coverage over most of the planet. EMM has three scientific objectives to (A) characterize the state of the Martian lower atmosphere on global scales and its geographic, diurnal and seasonal variability, (B) correlate rates of thermal and photochemical atmospheric escape with conditions in the collisional Martian atmosphere, and (C) characterize the spatial structure and variability of key constituents in the Martian exosphere. The EMM data products include a variety of spectral and imaging data from three scientific instruments measuring Mars at visible, ultraviolet, and infrared wavelengths and contemporaneously and globally sampled on both diurnal and seasonal timescale. Here, we describe our strategies for addressing each objective with these data in addition to the complementary science data, tools, and physical models that will facilitate our understanding. The results will also fill a unique role by providing diagnostics of the physical processes driving atmospheric structure and dynamics, the connections between the lower and upper atmospheres, and the influences of these on atmospheric escape.

Keywords EMM · Emirates · Mars · Mission · Hope · Atmosphere · Dynamics

1 Introduction

The Emirates Mars Mission (EMM), launched on July 20, 2020 at 01:58:14 GST (July 19, 2020 at 21:58:14 UTC) and entered Mars orbit on February 9, 2021, is the United Arab

The Emirates Mars Mission
Edited by Dave Brain and Sarah Yousef Al Amiri

Extended author information available on the last page of the article

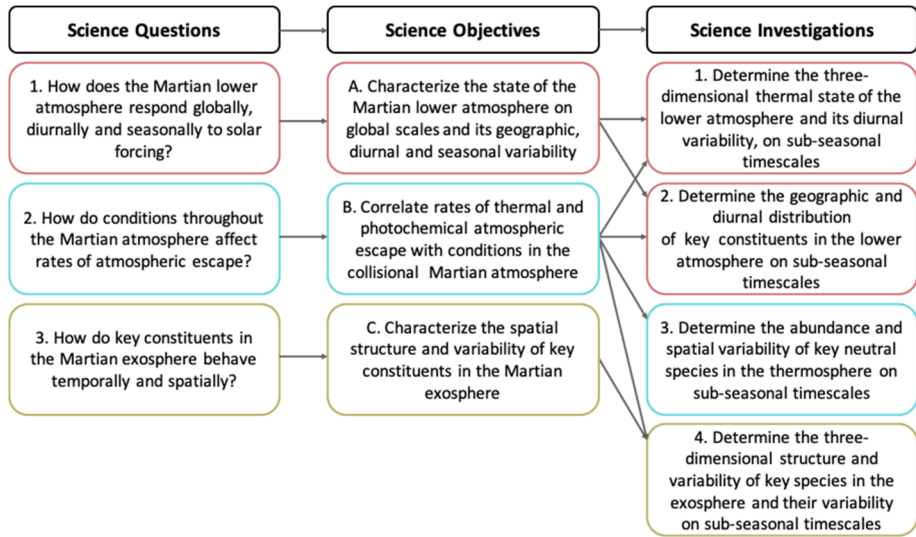


Fig. 1 EMM science questions mapped to EMM science objectives and investigations

Emirates' (UAE) first mission to Mars, and the Arab World's first mission to another planet. EMM is designed to study the dynamics of the Martian atmosphere on a global scale, and on both diurnal and seasonal timescales, furthering our understanding of Mars' atmosphere that has been limited by fixed geographical coverage and local time samplings. The mission will enable us to explore the atmospheric processes that drive diurnal variations, how energy is transferred from the lower-middle atmosphere to the upper atmosphere, and how lower atmosphere conditions are connected to the escape of atmospheric particles from Mars. The scientific motivation of EMM can be distilled to three motivating science questions leading to three associated objectives and four scientific investigations, seen in Fig. 1.

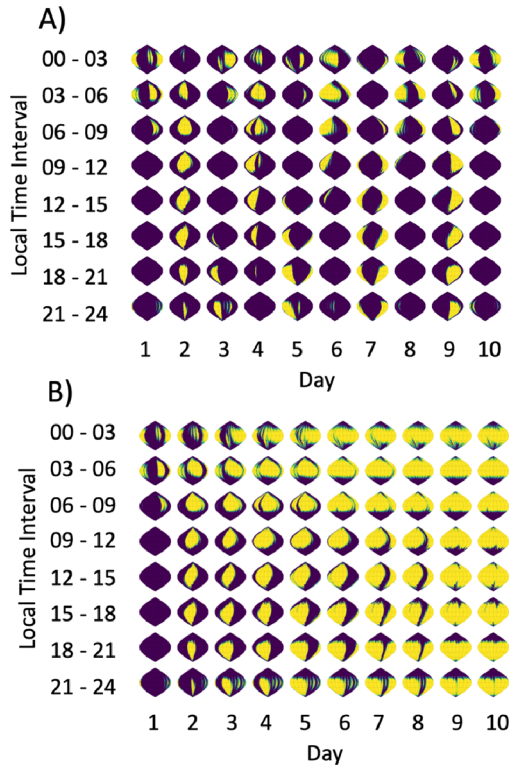
EMM will achieve these objectives with measurements from three scientific instruments: Emirates eXploration Imager (EXI), Emirates Mars InfraRed Spectrometer (EMIRS), and Emirates Mars Ultraviolet Spectrometer (EMUS).

EXI is a multi-wavelength radiation tolerant camera that consists of a double lens assembly to separate the ultraviolet (UV) and visible (VIS) optical paths and can take 12-megapixel images of the full Martian disk. Its UV lens system includes two channels, UV-C (245–275 nm) and UV-A (305–335 nm), to measure ozone and ice clouds respectively in the Martian lower atmosphere. Its VIS system includes Red (625–645 nm), Green (506–586 nm) and Blue (405–469 nm) bands to capture high resolution color images of Mars.

EMIRS is an interferometric thermal infrared spectrometer that will complement EXI in characterizing the lower atmosphere of Mars by taking measurements of infrared radiance and determining the distribution of lower atmospheric constituents such as dust, water ice and water vapor optical depths, in addition to Mars surface and atmospheric temperature profiles up to 50 km from the surface with vertical resolution of ~ 10 km. EMIRS will aid in better understanding the thermal state of Mars and its global circulation in terms of energy balance. EMIRS operates in the $6\text{--}40^+ \mu\text{m}$ range with 5 cm^{-1} and 10 cm^{-1} spectral sampling.

EMUS is a far ultraviolet spectrometer that will measure the variability of the Martian upper atmosphere. It is designed to measure emissions of hydrogen (H; Lyman alpha 121.6 nm

Fig. 2 The illustration in panel A shows a projected coverage for EMM individual observations per day and local time for a duration of 10 days for a starting date of May 23, 2021 (start of science phase). Each column is a day of observations. The observations are taken at different local times, and binned according to which row they land in. The yellow color indicates a good resolution coverage, the dark blue color indicates no observations, and the green indicates observations with fair resolution. Panel B shows how the observations accumulate in coverage. By Day 10, the majority of the local time and geographic state space has been imaged with sufficient resolution



and Lyman beta 102.6 nm), oxygen (O; 130.4 nm and 135.6 nm), and carbon monoxide (CO; Fourth Positive Group (4PG) band from 140–170 nm). EMUS spectral range is 100–170 nm, and it has multiple slit positions for science purposes that provide spectral resolutions of 1.3 nm and 1.8 nm.

EMM orbits Mars at an inclination of 25 deg, with a periapsis of 19,970 km and apoapsis of 42,650 km altitude, and an orbital period of 54.5 hours. The orbit enables EMM to have a combination of global geographic and local time coverage every 9–10 days, see Fig. 2, on diurnal and sub-seasonal timescale. The science phase will last for one Martian year (687 days, almost two Earth years), to collect data, with full geographic, diurnal and seasonal coverage, necessary to answer the science objectives of the mission. More information on the EMM mission (Amiri et al. 2021) and the three instruments (Jones et al. 2021; Edwards et al. 2021; Holsclaw et al. 2021) can be found in review papers within this special issue.

This paper will discuss the EMM science team's strategy for achieving closure on the science objectives introduced above, which can be summarized as (A) characterizing the state of the Martian lower atmosphere, (B) correlating the lower atmosphere conditions with rates of thermal and photochemical atmospheric escape, and (C) characterizing the spatial structure and variability of hydrogen and oxygen in the Martian exosphere. Section 2 provides a brief overview of the current state of Mars atmospheric science in these areas. Section 3 describes the key global circulation models and tools that will be used in addressing EMM scientific objectives. Sections 4, 5, and 6 discuss in detail the strategies for achieving objectives A, B, and C, respectively, in terms of planned analyses, data, and models to be used for each. Section 7 provides a summary that highlights the unique role EMM will play in answering open scientific questions and fulfilling needs of the Martian science community.

2 Current State of Mars Atmospheric Science

The Mars atmosphere can be divided into three regions based on distinctive characteristics: the lower atmosphere (up to 50 km), the middle atmosphere (50–100 km), and the upper atmosphere (above 100 km) (Smith et al. 2017). While the temperature in the lower atmosphere decreases with altitude, it remains relatively constant in the middle atmosphere, and generally increases with altitude in the upper atmosphere (Haberle et al. 2017).

Carbon dioxide (CO₂) dominates the bulk of Mars atmospheric composition with an average mixing ratio of 95.1%, with traces of mainly nitrogen (N₂), argon (Ar), oxygen (O₂), and carbon monoxide (CO) (Nier and McElroy 1977; Trainer et al. 2019). The dynamics of Mars' present-day lower atmosphere is characterized mainly by the behavior of CO₂, water vapor, and dust in response to solar and seasonal variabilities and their interaction with the surface (e.g. Barnes et al. 2017 and references therein). In contrast, dynamics in the thermosphere (100–200 km), are driven from two directions: from below by the heating and wave propagation from the lower atmosphere and from above by solar UV radiation heating and the heliospheric charged particle and magnetic field environment (commonly known as space weather) (Bougher et al. 2017). At the homopause (~100 km), the atmosphere transitions from a well-mixed state dominated by eddy diffusion to a more weakly-mixed state (i.e. thermosphere) where molecular diffusion dominates and constituents have separate scale heights. Above the exobase (~200 km) is the exosphere where collisions are extremely rare and particles move ballistically subject to gravity (Izakov and Krasicki 1977; Zurek et al. 2017). The characteristics of the upper atmosphere (i.e. thermosphere-exosphere) structure enables the understanding of Mars present-day escape rates and the processes which drove the transition of Mars from a thick to thin atmosphere in the past (Bougher et al. 2015).

Measurements from past missions like Mariner 9, Vikings 1 and 2, Mars Global Surveyor (MGS), 2001 Mars Odyssey, Mars EXpress (MEX), Mars Reconnaissance Orbiter (MRO), and Trace Gas Orbiter (TGO), have helped in characterizing and understanding the lower atmosphere and the global atmospheric circulation through studies of interactions between the thermal structure, active gases (water vapor) and active aerosols (clouds and dust) (e.g. see the reviews by Smith et al. 2017; Wolff et al. 2017; Clancy et al. 2017; Kahre et al. 2017; Montmessin et al. 2017).

The thermal structure of the lower atmosphere depends greatly on the surface temperature, dust content and aerosol dynamics. It is influenced by seasonal, latitudinal and “orbital seasons” caused by the relatively large difference between Mars' perihelion and aphelion distance from the Sun. The standard Martian seasons mainly drive changes in surface and atmospheric temperatures, more so at high latitudes, while the orbital seasons have greater impact on the surface and the atmospheric temperatures at low latitudes (Smith et al. 2017; Heavens et al. 2011). The thin atmosphere also allows optical radiation to reach the surface, significantly impacting the diurnal surface temperature cycle, thus also the near-surface atmospheric temperature (Kleinböhl et al. 2013; Martínez et al. 2017). Diurnal information on Mars' thermal state is limited primarily because previous spacecraft have mostly been in Sun-synchronous orbits that only sample two opposite local times (e.g. 2 AM/2 PM for MGS).

Dust plays a key role in Mars atmospheric dynamics. It is an abundant constituent on the Martian surface and in the atmosphere where it resides mainly in the lower-middle atmosphere. It acts as an absorber for solar radiation and emitter/absorber for infrared radiation thus strongly affecting the thermal structure of the Martian atmosphere (e.g. Gierasch and Goody 1972; Smith 2004; Kahre et al. 2017). Dust has somewhat regular seasonal and spatial patterns of influence with significant interannual variations that have been characterized by spacecraft observations (e.g. Smith 2004; Smith 2009; Montabone et al. 2015). Its

seasonal pattern can be divided into two main periods: (1) non-dusty season (solar longitude (L_s) $\sim 0^\circ$ - 135°) during northern spring/summer where column dust opacity is low, and (2) dusty season ($L_s \sim 135^\circ$ - 360°) during southern spring/summer where local, regional or global dust storms evolve varying in size and time (e.g. Smith et al. 2002; Smith 2004, 2019; Kahre et al. 2017; Kass et al. 2016).

Another key constituent in the lower atmosphere of Mars is water vapor. Water vapor is the main form of water in Mars' atmosphere and is important for understanding the overall Martian water cycle and has been observed using absorption bands in the thermal-IR and near-IR (e.g. Jakosky and Farmer 1982; Smith 2002; Smith et al. 2018; Montmessin et al. 2017). The global average water vapor column is about 10 precipitable microns (pr- μm), but the release of water from sublimation of the northern hemisphere seasonal cap leads to peak values of up to ~ 50 pr- μm during early northern summer. The corresponding maximum in the southern hemisphere spring/summer has a smaller amplitude of ~ 25 pr- μm . Vertical profiles of water vapor have been obtained by solar occultations (Maltagliati et al. 2011; Fedorova et al. 2020) revealing a very dynamic 3D structure and high supersaturation.

Water vapor condenses to form thin water ice clouds whose variations can play a major role in the radiative budget of the lower atmosphere (e.g. Clancy et al. 1996; Richardson et al. 2002; Madeleine et al. 2012). Ozone is anticorrelated with water vapor; as water vapor photodissociates in the atmosphere, it increases the abundance of odd hydrogen, which destroys ozone (Perrier et al. 2006). Ozone can be measured in the lower atmosphere and middle atmosphere through the Hartley Band absorption centered at 255 nm (Perrier et al. 2006; Clancy et al. 2016).

Previous Mars missions have revealed ample evidence of past liquid water on Mars surface in the form of ancient streambeds, precipitation-fed valley networks, flood channels and the presence of significant quantities of hydrated minerals such as phyllosilicates. These signs imply that Mars, in order to sustain liquid water on its surface, once had a thicker atmosphere. Atmospheric escape has been established to be one of the primary drivers of Mars climate evolution over solar system history (Jakosky et al. 2018). Studies have shown that hydrogen and oxygen, the building blocks of water, are the dominant neutral species that escape Mars today through mainly Jeans escape (thermal), and photochemical escape (non-thermal) consecutively (Brain et al. 2017; Lillis et al. 2015; McElroy 1972a). Mars atmospheric escape had been studied by many Mars missions including, but not limited to, Mariner 6, 7, 9, MEX, and Mars Atmosphere and Volatile Evolution mission (MAVEN).

Hydrogen is transported from the lower and middle atmosphere to the upper atmosphere through the water photodissociation process. As a hydrogen atom collides with other atoms and molecules in the upper atmosphere, it gains or loses kinetic energy. Those hydrogen atoms in the high-energy tail of the Maxwell-Boltzmann distribution have sufficient energy to travel to high altitudes, forming the hydrogen corona around Mars, or can escape the atmosphere entirely, if the atom has a velocity at or above the escape velocity (~ 5 km/s for Mars). Hydrogen loss to space was estimated recently by MAVEN at a rate of $\sim 1 - 11 \times 10^{26} \text{ s}^{-1}$ with a strong seasonal variation (Halekas 2017; Rahmati et al. 2018; Chaffin et al. 2018).

Atomic oxygen is most abundant species in the upper thermosphere and lower exosphere of Mars. It has two main populations: a thermal or 'cold' population, and an energetic 'hot' population originating from, the exothermic dissociative recombination of O_2^+ ions in the ionosphere. A significant fraction of these hot oxygen atoms have sufficient energy to escape the collisional atmosphere forming the oxygen corona around Mars. Oxygen loss to space was estimated recently by MAVEN at a rate of $\sim 5 \times 10^{24} \text{ s}^{-1}$ (Jakosky et al. 2018).

The thermosphere overlaps the lower boundary of the exosphere and is the channel through which particles from the lower atmosphere are energized and can ultimately escape. Past authors have shown that the thermosphere is significantly affected by conditions in both Mars' lower atmosphere and the near-space environment (Lillis et al. 2015; Mayyasi et al. 2018). In the lower atmosphere, dust storms strongly affect the upper atmosphere, impacting its composition and temperature across all latitudes. These dust phenomenon occur primarily over $L_s \sim 180\text{--}330^\circ$ in the form of regional or global scale dust storms that have a strong impact on the upper atmosphere (e.g. Keating et al. 1998; Bougher et al. 1999; Fang et al. 2020; Elrod et al. 2019; Jain et al. 2020). Small dust storms are also known to occur over $L_s \sim 20\text{--}120$, and likewise have a substantial upper atmosphere impact (e.g. Withers and Pratt 2013; Felici et al. 2020). The space weather associated with solar activities like solar flares, solar energetic particles (SEP), and coronal mass ejection (CME) can heat and ionize the upper atmosphere, decreasing the abundance of hydrogen by $\sim 25\%$, intensifying the hot oxygen density in the thermosphere by $\sim 15\text{--}45\%$, and temporarily increasing the rate of escape for both hydrogen and oxygen, by up to 20% (Mayyasi et al. 2018; Lee et al. 2018).

EMM aims to further our understanding of diurnal, global, and seasonal variations of the Martian atmosphere, drawing a clearer picture of Mars atmosphere dynamics. EMM will characterize the lower atmosphere through measurements of temperature profiles, surface temperature, water ice, dust and ozone column integrated depths, as well as water vapor column abundance. It will study the escape rates of hydrogen and oxygen in the exosphere by making measurements of hydrogen and oxygen emissions. And finally, it will study the connection between the lower atmosphere and the upper atmosphere through the derivation of the column abundances of oxygen and carbon monoxide in the thermosphere. Figure 3 illustrates Mars atmospheric layers mapped to EMM measurements.

3 Key Global Circulation Models and Tools

The scientific analyses needed to address EMM science objectives from the mission data sets require the use of global circulation models. Specifically, we will employ the LMD-MGCM to infer unobservable quantities (at least by EMM) such as winds or values at local times not observed, to compare with derived or retrieved quantities, or to understand the behavior exhibited by the data. EMM will also utilize an advanced visualization tool for the three instruments' data, called JMARS (<http://jmars.asu.edu>), to visualize and cross-link datasets of disparate temporal and spatial scales ultimately permitting advanced data discovery and analysis. Sections 3.1 and 3.2 describe LMD-MGCM model and JMARS respectively.

3.1 LMD Mars General Circulation Model (LMD-MGCM)

The Laboratoire de Météorologie Dynamique Mars General Circulation Model (LMD-MGCM) is a three-dimensional model of the Martian atmosphere from the surface up to 240 km in the exosphere and is considered the first Mars GCM that couples the lower atmosphere to the upper atmosphere providing valuable atmospheric transfer information (Forget et al. 1999; Millour and Forget 2018; Angelats i Coll et al. 2005). The model simulates the Martian climate by solving fluid mechanics and meteorology equations over a sphere in order to calculate the dynamical behavior of the atmosphere. It integrates these processes over time to track their evolution (Forget et al. 1999) and include complete models of the dust, water and CO_2 cycles as well as the photochemistry. Variables that describe and regulate

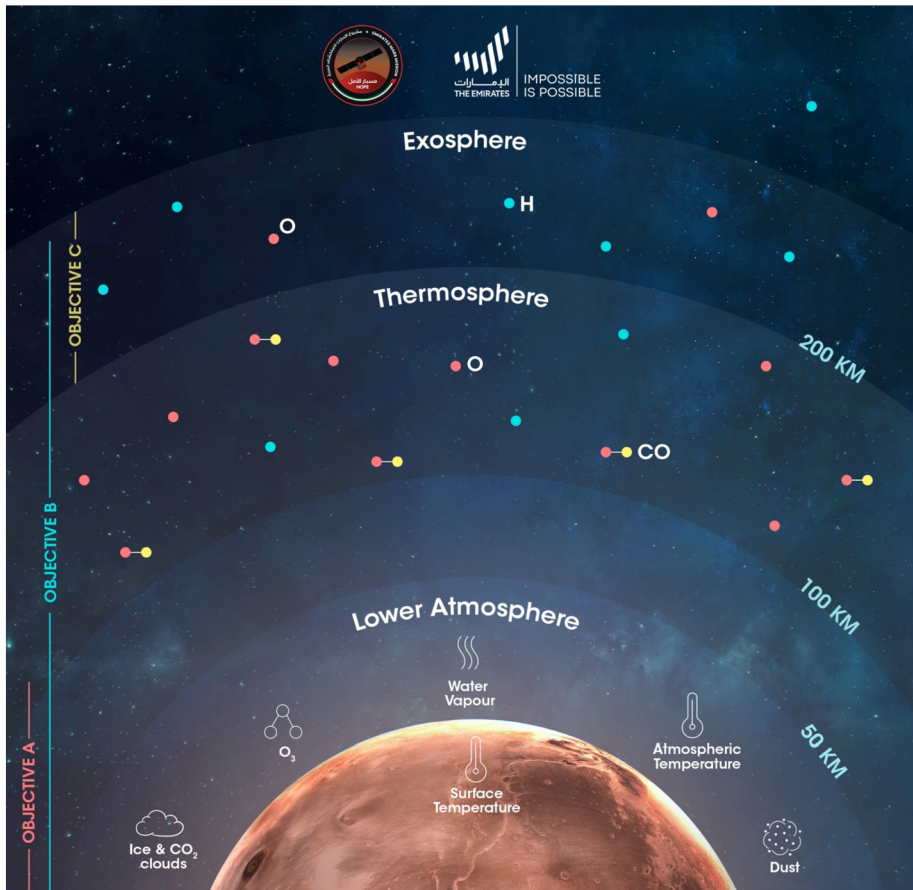
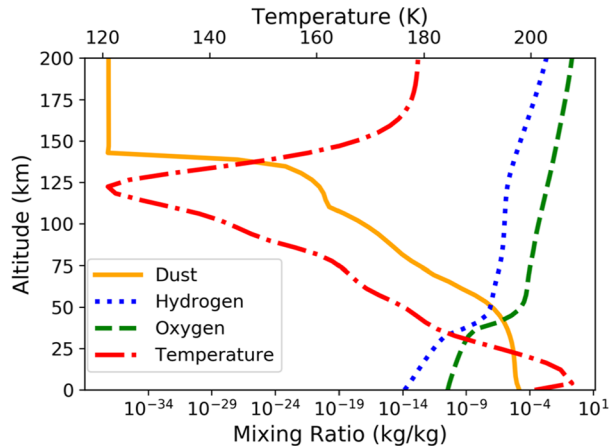


Fig. 3 Illustration of Mars atmospheric layers mapped to EMM objectives and measurements

the climate of Mars are allowed to evolve through the calculations in the model over each time-step (Millour and Forget 2018). The LMD-MGCM typically employs a 64×48 grid, which provides for a longitudinal resolution of 5.625 degrees and a latitudinal resolution of 3.75 degrees. However, dynamics that occur at scales smaller than a grid cell, like turbulence, convection or gravity waves, are accounted for in the model through parameterization (Forget et al. 1999).

In the LMD-MGCM, the neutral atmosphere is simulated by including the transport, diffusion, and 92 chemical reactions of 25 different chemical species, and the model accounts for UV heating, photodissociation effects, thermal and viscosity conduction and molecular diffusion to simulate cooling that occurs in the upper atmosphere to balance UV heating (Angelats i Coll et al. 2005; González-Galindo et al. 2009, 2013). The model simulates the radiative transfer through atmospheric layers taking into account aerosol (dust and ice) radiative effects and CO₂ radiative transfer (Madeleine et al. 2011, 2012). The surface properties in the LMD-MGCM are modeled based on the derived thermophysical properties of Martian soil (Forget et al. 1999) (e.g. thermal inertia, albedo etc.), while most fields are calculated based on fundamental equations, the LMD-MGCM usually takes as an input daily

Fig. 4 Example of an LMD-MGCM output for 10 days (sol 510-sol 520) of the MY34 southern summer dust storm which shows the average temperature vertical, and the vertical distribution of dust, oxygen, and hydrogen mixing ratios, both over all longitudes and latitudes



maps of the dust columns derived from the available observations over different Mars Years (Montabone et al. 2015).

Since EMM cannot observe all locations and all local times simultaneously, the LMD-MGCM can support EMM observations by providing data for times and locations that are not covered by EMM instruments as seen in Fig. 4 in which vertical profiles of temperature, dust, hydrogen, and oxygen are plotted from the surface to 200 km. In practice the LMD-MGCM will be used to analyze the data in two major ways. First, it gives a context and predictions against with EMM observations can be compared (especially where no other instruments have ever observed), providing physical explanations for the observed phenomenon when the model is valid or, even more interesting, highlighting unexpected behavior and possibly new processes when the model does not match the observations. Second it can be used to help reconstruct the actual state of the observed atmosphere on the basis of the observations, for instance by calculating the winds corresponding to the observed temperature fields. This can notably be done in an optimal way using data assimilation techniques (See Sect. 4.4).

3.2 The Java Mission-Planning and Analysis for Remote Sensing (JMARS)

The Java Mission-Planning and Analysis for Remote Sensing (JMARS) is an advanced java-based software package developed by Arizona State University's Mars Space Facility, to provide scientists, instrument team members, and the general public a mission planning and scientific data-analysis tool that can be used to study different planetary systems (Christensen et al. 2009). JMARS graphical user interface provides access to many Mars related scientific products, such as, image footprints, rasters, local mosaics, vector-oriented data, numerical and graphical maps, all of which are derived from instruments of different National Aeronautics and Space Administration's (NASA) missions, including Viking 1 and 2 Orbiters, MGS, 2001 Mars Odyssey, MEX, and MRO (Dickenshied et al. 2014; Christensen et al. 2009) as well as a host of derived data products. In addition, other functionality such as running models such as the KRC thermal model (Kieffer 2013) or querying complex database related dataset such as the LMD-MGCM can interface with measured data and provide preliminary mechanisms to make scientific interpretations.

Using JMARS, multiple datasets of interest can be queried based on user desired observational parameters, data quality, geographical location and time period, among a host of

other parameters. These data can then either be visualized in context with one another, or cross-linked with intersecting products from other modules or instruments from different missions for the same study scenario (Dickenshied et al. 2014).

Science data returned from the EMM's three instruments (EXI, EMIRS and EMUS) once in the science orbit, will be hosted in JMARS software package, whereby data can be displayed, analyzed independently, compared across datasets, and validated. Analysis performed using JMARS on the measurements derived from EXI and EMIRS for the lower atmosphere, and from EMUS for the upper atmosphere includes, but are not limited to, identifying possible patterns and behaviors in the global snapshot of the atmosphere, comparing products of similar data quantities, conducting spatial and temporal comparisons with data from other missions or modules, correlating conditions in the lower atmosphere with those in the upper atmosphere, and analyzing responses of selected episodic events. Figure 5 illustrates EMIRS observation footprints mapped in 2D and in 3D using JMARS.

4 Objective A: Characterize the State of the Martian Lower Atmosphere on Global Scales and Its Geographic, Diurnal and Seasonal Variability

EMM Objective A focuses on characterizing the state of the lower Martian atmosphere and the processes that are driving the global circulation to improve our understanding of the energy balance in the current Martian climate. Understanding the energy balance will help in identifying the sources and sinks of energy globally and how the lower atmosphere responds to solar forcing diurnally and seasonally. To meet objective A science, we plan to (A1) merge EMIRS and EXI observations into a combined multi-dimensional snapshot of the global atmosphere, (A2) compare products of similar data quantities between EXI and EMIRS, (A3) conduct spatial and temporal comparisons to LMD-MGCM and other observations or spacecraft datasets, and ultimately (A4) produce a reference climatology using meteorological data assimilation techniques. The following sections detail these analyses and the data and models (if any) needed for each. Table 1 summarizes required data, physical models and tools for each analysis.

4.1 A1: Merge Observations into a Combined Multi-Dimensional Snapshot of the Global Atmosphere

The data from the EMIRS and EXI instruments will help in understanding the energy balance in the current Martian climate and how the lower atmosphere responds to solar forcing diurnally and seasonally. Individual observation sets from EMIRS and EXI will be used to retrieve temperature, dust, water ice, ozone, and water vapor in the lower atmosphere independently and then will be deployed on JMARS, for visualization, to create a multi-dimensional snapshot of the global atmosphere every ~ 10 days. The 10-day time interval will provide maps that can be accessed through queries, and which will have adequate spatial and diurnal coverage to understand the general behavior and patterns of the retrieved values. Visible images will be used to constrain the surface albedo, an important part in the atmospheric thermal balance, and also the location of regional-scale to global-scale dust events, in combination with EMIRS retrieved dust optical depths.

4.2 A2: Compare Products of Similar Data Quantities Between EXI and EMIRS

Atmospheric aerosols in the Martian atmosphere interact with solar and thermal radiation and thereby drive the Mars climate system, particularly through its overall energy balance

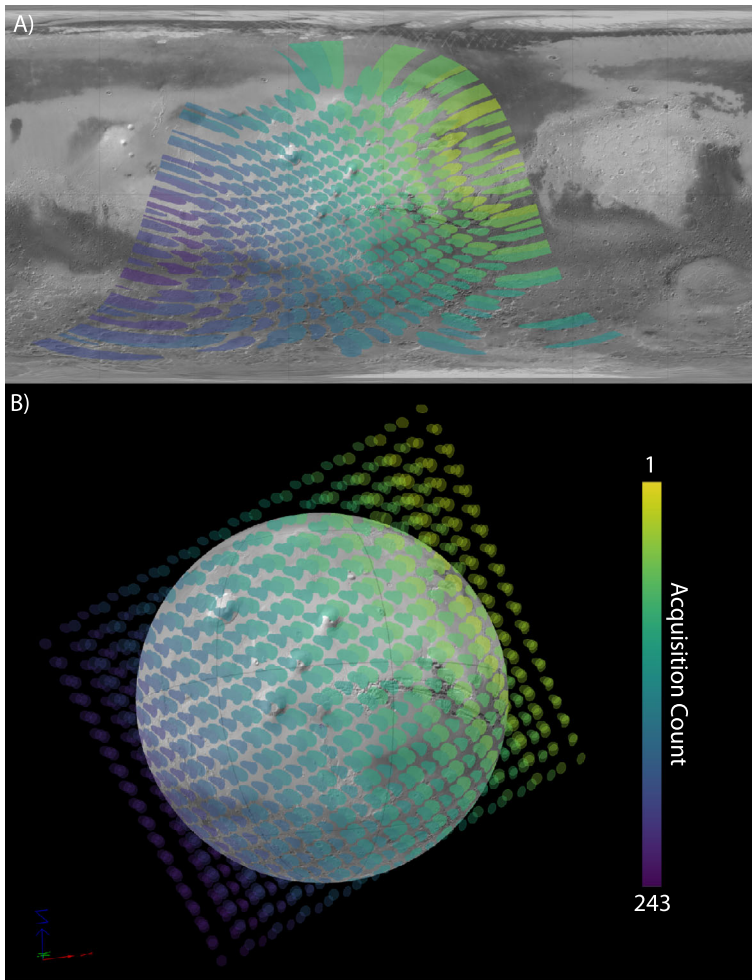


Fig. 5 EMIRS footprints highlighted by acquisition count (from 1 to 243) shown on top of a TES Lambert Albedo (Christensen et al. 2001) overlay on MGS-Mars Orbiter Laser Altimeter (MOLA) Shaded Relief (Smith et al. 2001) in both mapping mode (panel A) and 3D mode (panel B) as displayed in JMARS. The data represent a spacecraft altitude of 31,400 km and the images are centered on $\sim 0^\circ$ N and $\sim 270^\circ$ E

(e.g. Wolff et al. 2017 and references therein). Water ice cloud aerosols in the atmosphere of Mars are a topic of considerable interest due to their effect on Martian general circulation and water cycle (Richardson et al. 2002); thus understanding the microphysical properties of water ice, such as particle size, is important, as it is the key to correctly calculate its contribution to the energy budget (Guzewich and Smith 2019). We plan to constrain the average particle size of water ice using the visible-to-infrared ratio obtained from a combination of EXI derived water ice optical depth at 320 nm, retrieved from the observed radiance in the 315–325 nm range, and EMIRS retrievals of ice optical depth at 12 μm . In addition to the analysis approach explained in Sect. 4.1, EMM will sample the Martian lower atmosphere on both greater and lesser temporal and spatial scales, to examine the behavior in “special” regions and events that are known for their ability to influence the overall energy bal-

Table 1 Mapping of objective A analyses to needed EMM data, and other data, tools, and physical models

Objective A analyses:	(A1)	(A2)	(A3)	(A4)
<i>EMM Data</i>				
EMIRS	Atmospheric and surface temperatures	*	*	*
	Dust optical depth at 9 μm	*	*	*
	Water vapor column abundance at 25–40 μm	*	*	*
	Ice optical depth at 12 μm	*	*	*
EXI	Ice optical depth at 320 nm	*	*	*
	Ozone column abundance at 260 nm	*	*	*
	Visible image of Mars	*		
EMUS	Thermospheric oxygen and carbon monoxide column			
	Density of hydrogen and oxygen corona			
<i>Others (related to objective A)</i>				
Data	MGS/MRO/MEX Retrievals		*	*
Tools	JMARS Visualization	*	*	*
Models	LMD-MGCM		*	*
	Data Assimilation Scheme			*

ance/budget (e.g. orographic clouds, dust storms). Although this analysis is not a key driver in achieving EMM objective A, understanding it will help constrain the current state of the atmospheric circulation, and identify the processes driving global circulation. The JMARS visualization and analysis tool will be of value to study and examine these influences.

4.3 A3: Conduct Spatial and Temporal Comparisons to GCM and Other Observations or Spacecraft Datasets

Conducting spatial and temporal comparisons between EMIRS and EXI's retrievals and other data from previous missions or models are of tremendous benefit. It (1) furthers our knowledge in processing EMM observations prior and during the science mission; it (2) helps interpolating and interpreting EMM data by placing them in similar context and state of other data sets; it (3) aids in identifying parameters, within an observation, that require new modeled physical processes to precisely replicate its observed behavior and enhance the accuracy of developed retrieval algorithms; and it (4) facilitates new scientific discoveries that could be made when explaining unexpected behavior and inconsistency between the model and the observed data.

The data retrieved from EMIRS and EXI including atmospheric and surface temperatures, water ice optical depths, dust optical depth, and water vapor and ozone column abundances, will be compared with the LMD-MGCM output that will be binned and sampled similar to EMM mission's observation taking into consideration diurnal sampling as well. Also, derived products such as the water ice aerosol particle size, explained in Sect. 4.2, will be compared to LMD-MGCM results with proper geometric-averaging treatment of the latter's results to account for the column-integrated nature of the aerosol retrievals. Retrieved constituents will also be compared, when possible, to previous missions' retrievals, such as MGS, 2001 Mars Odyssey, MEX, MRO, and TGO, to gain similar insight. The JMARS visualization and mission planning tool will also be used for sampling different temporal and

spatial scales and for mapping activities based on EMIRS and EXI concept of operations. It can facilitate the comparison and promote novel science discoveries during the analysis.

4.4 A4: Produce a Reference Climatology Using Meteorological Data Assimilation Techniques

Both surface and atmosphere properties are expected to vary diurnally, spatially, and seasonally. However, our current understanding is limited by the relative lack of local time coverage in existing observational datasets which is critical as diurnal variations in Mars' atmosphere are considerable (e.g. Navarro et al. 2017; Smith et al. 2017).

Data assimilation techniques will be used to produce a comprehensive dataset of Martian atmospheric circulation (so-called "maps without gaps"), which can be used to study Mars' climatology, atmospheric events, and other phenomena (Lewis et al. 1996; Navarro et al. 2017). Using these techniques, we will optimally combine observational data from EMIRS and EXI with numerical (theoretical) models contained in the LMD-MGCM (Forget et al. 1999), to replicate and reanalyze Mars atmospheric circulation over the course of EMM's science mission (see Fig. 6). Data assimilation techniques are vital in order to obtain a full picture of the global climate, as they estimate the atmospheric state in sparsely-observed regions by combining a model prediction of the atmospheric state in that region with observations from other, densely-observed regions. They can also estimate quantities that cannot be retrieved using EMM observations (such as wind speed and direction) because the model adjusts itself to remain consistent with observed values while maintaining an internal balance between its simulated quantities.

To verify the accuracy of our Mars maps, JMARS will be used to validate EMM's lower atmosphere results through the addition of a layer for LMD-MGCM output in JMARS, and then comparing the results with EMM observations and other existing independent observations.

5 Objective B: Correlate Rates of Thermal and Photochemical Atmospheric Escape with Conditions in the Collisional Martian Atmosphere

EMM Objective B focuses on better understanding the processes that drive atmospheric escape, by correlating the rates of thermal and photochemical atmospheric escape with conditions in the collisional Martian atmosphere (i.e. below the exobase). Specifically, the upper atmosphere measurements from EMUS and the lower atmosphere measurements from EXI and EMIRS will be used in concert through the following analyses: (B1) correlating conditions in the lower atmosphere with those in the upper atmosphere, (B2) comparing escape rate variations (and other exospheric properties) with thermospheric conditions, and (B3) analyzing the response of the atmosphere to episodic events which are: (B3.1) dust storm, (B3.2) solar flare, (B3.3) solar energetic particle events and coronal mass ejections, (B3.4) polar ice cap variability, and (B3.5) dust deposition and removal events. The following sections detail these analyses and the data and models (if any) needed for each. Table 2 summarizes required data, physical models and tools for each analysis.

5.1 B1: Correlate Conditions in the Lower Atmosphere with Those in the Upper Atmosphere

Upper atmosphere variables that EMM will measure (e.g. exobase hydrogen or oxygen density or temperature, or thermospheric mixing ratios) may increase or decrease in response

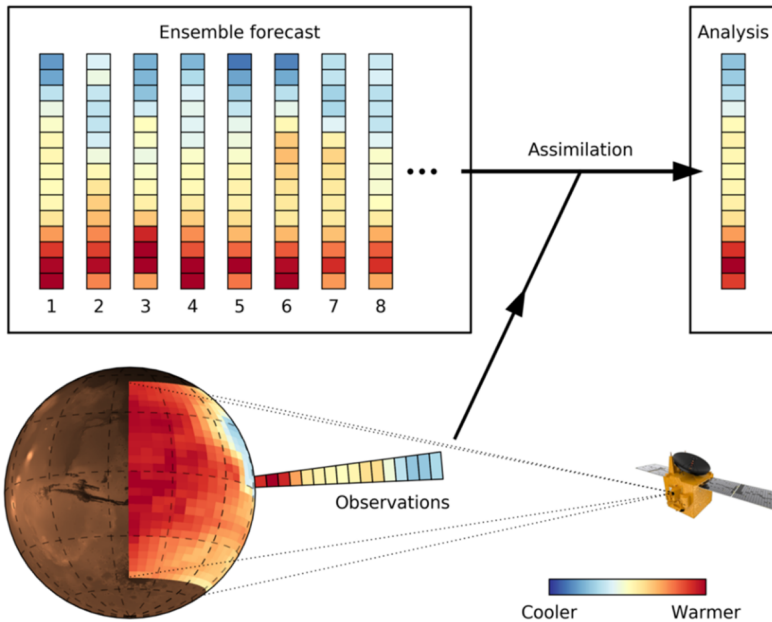


Fig. 6 Schematic illustrating data assimilation using EMM observations. To produce an atmospheric temperature “analysis” in a particular atmospheric column, first we make several forecasts of the temperature in the column using the LMD-MGCM; the spread of values over the forecast ensemble members sets the uncertainty in the prediction. Observations from EMM (in this case a vertical temperature profile retrieved from EMIRS spectra) are then combined with the forecast using data assimilation to produce the analysis. (Topography is from MGS-MOLA; the vertical distance in the atmospheric profile is greatly exaggerated)

to changes in the lower atmosphere. Lower atmosphere conditions include temperature, water abundance, and dust content, that could propagate to higher altitudes and affect upper atmosphere constituents.

A simple correlation of changes, empirically or with the aid of atmospheric models, that occur at the two locations (i.e. altitudes or geographic locations) in the atmosphere could indicate a causal effect between physical quantities. For this analysis, lower atmosphere data, from EMIRS and EXI, which are ice optical depth, ozone column abundance, dust optical depth, water ice optical depth, water vapor abundance, atmospheric temperature, surface temperature, and emissivity will be correlated numerically with upper atmosphere data, from EMUS, which are exospheric hydrogen and oxygen densities. A quantitative analysis of the likelihood of a lower atmosphere quantity or event covarying with an upper atmospheric quantity or event will be conducted. Strong correlations will suggest a physical link between observed quantities, but cannot be confirmed unless compared with future EMM observations, previous and future spacecraft measurements, and theoretical models to verify if an underlying physical mechanism is the likely cause of the correlation. Predicted variability will be modeled in the upper atmosphere in response to lower atmospheric driving and boundary conditions, and will be compared, in magnitude, with the observed variation from the data to determine when upper atmospheric variations should be linked to lower atmospheric changes to investigate the candidate mechanisms more thoroughly.

One-dimensional photochemical models will be used to provide context for the lower atmosphere and upper atmosphere connection by modeling vertical effects. In addition, LMD-MGCM output can be compared to EMM observations of the upper and lower atmosphere

Table 2 Mapping of objective B analyses to needed EMM data, and other data, tools, and physical models

Objective B Analyses:	(B1)	(B2)	(B3.1)	(B3.2)	(B3.3)	(B3.4)	(B3.5)
<i>EMM Data Products</i>							
EMIRS Atmospheric and surface temperatures	*		*			*	*
Dust optical depth at 9 μm	*		*				
Water vapor column abundance at 25–40 μm	*						
Ice optical depth at 12 μm	*						
EXI Ice optical depth at 320 nm	*						
Ozone column abundance at 260 nm	*						
Visible image of Mars						*	*
EMUS Thermospheric oxygen and carbon monoxide column	*	*		*			
Density of hydrogen and oxygen corona	*	*		*			
<i>Others (related to objective B)</i>							
Data EMUS derived escape rates		*	*	*	*		
EUV irradiance at Mars				*			
MAVEN Particle and fields data					*		
Tools JMARS Visualization	*		*			*	*
Models LMD-MGCM	*		*	*	*	*	*
1D photochemical model	*						
Thermospheric H, O production models		*			*		
ENLIL Space Weather Model (optional)					*		

to provide context to the observed data; through data assimilation, lower atmosphere observations from EMM data can be used as inputs to the model to observe middle atmospheric reactions and compare upper atmospheric reactions to EMM observations of the upper atmosphere. Furthermore, the analysis will benefit from information about the middle atmosphere that is not available from EMM and can be obtained, if needed, from models or other missions. This includes MRO-Mars Climate Sounder (MCS) temperatures that reach 80 km at 3 a.m./3 p.m., TGO solar occultations that provide dust, water vapor, and other molecules reaching 100 km at the terminator (6 a.m./6 p.m.), as well as MAVEN-Imaging UltraViolet Spectrograph (IUVS) retrievals of CO_2 , O_2 , and O_3 vertical profiles from stellar occultations and column abundances of O_3 from disk imaging.

5.2 B2: Compare Escape Rate Variations with Thermospheric Conditions

The thermosphere is strongly coupled with both the lower atmospheric conditions (Sect. 4) and the exosphere of Mars, making it the collisional and transitional region of the atmosphere (Bougher et al. 2015). In the thermosphere, atoms transfer energy through collisions, depending on their energy; they either stay in the thermosphere or escape to the exosphere (Lee et al. 2015). Therefore, it is important to analyze the influence of thermosphere dynamics and energetics on hydrogen and oxygen escape rates. In this analysis, EMM's thermospheric data will be cross-correlated to determine the link between thermosphere physical parameters (e.g. mixing ratios of O and CO) with hydrogen and oxygen escape rates. We

will quantitatively determine the likelihood that a thermospheric physical parameter has an effect on the structure of oxygen and hydrogen in the exosphere.

For this science analysis, we will rely on EMUS data products, which are mixing ratios of O and CO derived from the OI 135.6 nm and CO4PG bands brightnesses respectively, as well as exospheric hydrogen densities (Lyman alpha 121.6 nm, Lyman beta 102.6 nm) and exospheric oxygen densities (130.4 nm). We will use models simulating the interaction of hot oxygen and hot hydrogen with the thermosphere's key constituents, leading to their escape to the exosphere. Model utilization is necessary, as correlations between the thermospheric parameters on hydrogen and oxygen escape rates may not be solely dependent on one another and other physical mechanisms of the atmosphere may contribute. Hydrogen Lyman alpha is also an optically thick emission, where its emitted photons scatter across all altitudes presenting significant challenges and uncertainty in its interpretation alone and making it highly model-dependent (Chaffin et al. 2018). Therefore, we will use hydrogen Lyman beta emission as well as other EMUS observables to reduce this model dependence. Modeling results will be compared with EMM's observations to analyze the magnitude of variation between both outputs as well as evaluate the scale and response of hydrogen and oxygen escape.

5.3 B3: Episodic Events Studies and Their Responses

The linkage between the lower atmosphere and upper atmosphere of Mars is important in understanding the overall dynamics and atmospheric processes that affect the escape rates. There are a number of natural phenomena and episodic events (e.g. dust storms and solar events) that occur at Mars that can alter the lower atmosphere briefly and significantly on daily, seasonal or even annual timescales. These effects can cause disruption in the upper atmosphere over some time. Monitoring and studying these events and their physical processes will aid in understanding the lower-upper atmospheric connections and correlating rates of thermal and photochemical atmospheric escape. These analyses will be supported by EMM data from all three instruments as well as physical models for the Martian atmosphere, and data from other missions.

5.3.1 B3.1: Dust Storm Effect on Escape Rates

With Mars' dry environment dominated primarily by aeolian activity, regional to global scale dust storms are a common occurrence (e.g. Cantor et al. 2001; Malin et al. 2010; Cantor et al. 2019). Mars dust storms commonly occur during the southern hemisphere spring and summer seasons (e.g. Kahre et al. 2017). These dust storms occur through wind related processes and they last from weeks to months covering the entire planet (Zurek 1982; Zurek and Martin 1993). The wind-related processes encourage the development of local dust storms, which commonly have a limited occurrence scale in terms of size and duration as well as having low intensity of dust opacity in the area. These local dust storms can merge to develop into a continent-sized regional dust storm (Martin 1974; Fang et al. 2020) as seen in Fig. 7. The effects of such storms affect the balance by causing perturbations in the temperature, wind and density of the lower and also the upper atmosphere (Fang et al. 2020). Although the vertical transport of the dust can reach up to 80 km in the upper atmosphere, the impact is indirectly affecting the coupling between lower-upper atmosphere as a result modifying the escape of Hydrogen and Oxygen from the exobase region (Bougher et al. 1997; Keating et al. 1998; Qin et al. 2019; Elrod et al. 2019; Jain et al. 2020; Fang et al. 2020). Other studies (e.g. Leovy et al. 1973; Davies 1979; Montabone et al. 2005) have also

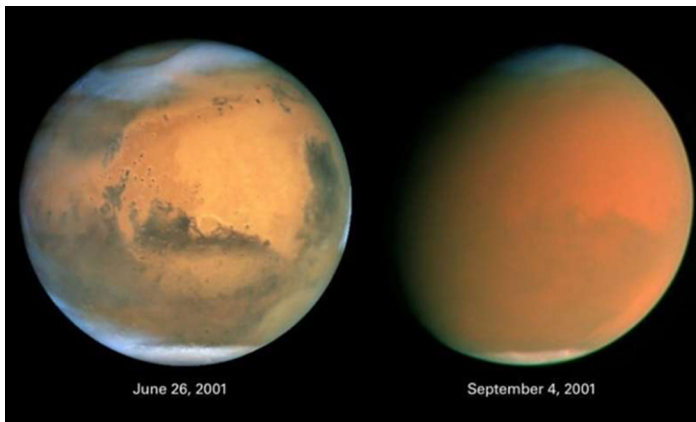


Fig. 7 Comparison of Mars before and during a global dust storm, as captured by the Hubble Space Telescope (HST) in 2001 (Credit: NASA/ESA and the Hubble Heritage Team STScI/AURA, J. Bell (Cornell), P. James (U. Toledo), M. Wolff (SSI), A. Lubenow (STScI), J. Neubert (MIT/Cornell))

shown that dust storms have great effect on atmospheric densities, temperature variabilities and wind flow in the Martian atmosphere dynamics. The observational study by Withers and Pratt (2013) done by analyzing the upper atmospheric effect show that even a small dust event can perturb the balance and can include nearly all latitudes. Observations from Mars Year (MY) 28 (Heavens et al. 2018; Clarke 2018; Fedorova et al. 2018) and MY 34 (Aoki et al. 2019; Fedorova et al. 2020) global dust storms provided evidence of enhanced water vapor transport to the middle atmosphere leading to an increase rate of water loss from the Martian atmosphere.

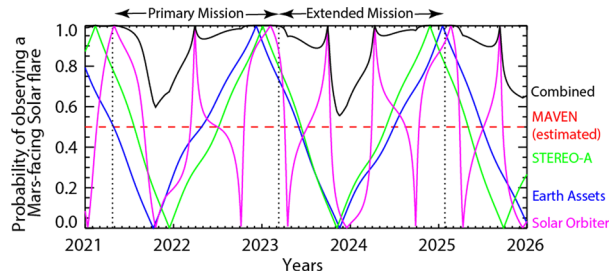
Using the LMD-MGCM, the behavior of dust storm events can be studied by providing the theoretical expectations necessary to link between dust storms and atmospheric conditions up to the exobase. Data from EMIRS measurements of temperature and dust optical depth will support this analysis.

5.3.2 B3.2: Solar Flares Effect on Escape Rates

Solar flares are impulsive, sudden releases of extreme ultraviolet and x-ray radiation from localized regions on the solar disk, associated with magnetic field reconfigurations within solar active regions, with durations of typically <2 hours (e.g. Fletcher et al. 2011). When flare photons impact Mars, they cause several effects: (1) significant heating in the thermosphere (Elrod et al. 2018; Fang et al. 2019; Jain et al. 2018), (2) increased ionization at all altitudes (Thiemann et al. 2018) but concentrated typically below 130 km (Xu et al. 2018), resulting in (3) increased photochemical escape of oxygen (Lee et al. 2018; Thiemann et al. 2018).

EMUS will observe the response of the Martian thermosphere, exosphere, and neutral escape rates to such flares. This analysis requires information on the timing and intensity of flares impacting Mars. While EMM does not carry a solar extreme ultraviolet (EUV) or x-ray detector, we will rely on a range of NASA and European space agency (ESA) assets to provide this information. Our primary source will be the MAVEN Extreme Ultraviolet Monitor (EUVM) (Eparvier et al. 2015), which provides solar EUV irradiance into wavelength ranges (17–22 nm and 121.6 nm) from MAVEN's $\sim 200 \times 4000$ km elliptical orbit around Mars. However, MAVEN experiences eclipses and must point away from the Sun regularly

Fig. 8 Probability of observing a Mars-facing solar flare by MAVEN and three different heliospheric observation points during the EMM primary and extended missions



to transmit and/or relay data to Earth (Jakosky 2020), resulting in $\sim 50\%$ coverage of solar activity.

If a flare is unobserved or incompletely observed by MAVEN, EMM will rely on other spacecraft around the Solar System monitoring solar EUV. Two Earth-orbiting spacecraft can provide high-quality flare data. First, the NASA Solar Dynamics Observatory's Atmospheric Imaging Assembly (AIA) (Lemen et al. 2012) observes the Sun in many EUV wavelengths, and can pinpoint the location of flares on the Sun's surface; simple geometry will tell us whether a given flare was visible from Mars. The flare's spectrum is provided by the Extreme Ultraviolet Variability Experiment (EVE) (Woods et al. 2012). Also orbiting Earth is the National Oceanic and Atmospheric Administration (NOAA) Geostationary Operational Environment Satellite (GOES), whose Solar Ultraviolet Imager (SUVI) can similarly pinpoint flare location, with flare spectra provided by the Extreme Ultraviolet and X-ray Irradiance Sensors (EXIS) or similar sensors are planned to be operational until at least 2035.

Away from Earth are two more important assets: (1) the NASA STEREO-A spacecraft in a circular heliocentric orbit close to 1 AU, drifting with respect to Earth, and (2) the ESA Solar Orbiter spacecraft in a smaller elliptical orbit around the Sun. While STEREO-A observes the Sun with its Extreme Ultraviolet Imager (EUVI) (Aschwanden et al. 2014), Solar Orbiter detects and pinpoints flares all the time with its Spectrometer Telescope for Imaging X-rays (STIX (Krucker et al. 2019)), though EUV spectra (from the Extreme Ultraviolet Imager (Rochus et al. 2020)) may not be available for all flares due to telemetry limitations (Müller et al. 2020). Since the orbits of Earth, Mars, STEREO, and Solar Orbiter are known, we can calculate the likelihood of a Mars-impacting solar flare being observed by at least one of these spacecraft during the EMM primary and extended mission. As shown in Fig. 8, the likelihood is usually very high that at least one of these assets will detect a Mars-facing solar flare, although the observation probability drops to $\sim 60\%$ in late 2021 and late 2023.

5.3.3 B3.3: Solar Energetic Particle (SEP) and Coronal Mass Ejection (CME) Effects on Escape Rates

Coronal Mass Ejections (CMEs) are large-scale eruptions on the solar disk that propel typically billions of tons of hot plasma outward into space at speeds up to 2000 km/s (Chen 2011). While much of the research of the effect of CMEs has concerned their effects on plasma escape from Mars (e.g. Curry et al. 2015), which EMM will not measure, we expect large CMEs to potentially produce dramatic temperature enhancements in the thermosphere (Fang et al. 2013), which should be visible as increases in FUV brightness at 135.6 nm. An observational study conducted in 2017 with regards to CME effect on Mars showcases the result of the event on the upper atmosphere. The flow of energy enhanced the emissions of hydrogen Lyman alpha in the upper atmosphere. This impacted the abundance of hydrogen by decreasing the amount by almost 25% and increasing the escape rate through the increase

in temperature in the exosphere (Mayyasi et al. 2018). Our primary source of data on coronal mass ejections will be magnetic field data from MAVEN and suprathermal (i.e. ~ 10 eV to 20 keV) ion and electron data from both MAVEN and Mars Express, both of which orbit Mars in elliptical orbits which take them into the upstream solar wind and thus allow them to detect CMEs.

Solar energetic particles (SEPs) are defined as high-energy (typically >20 keV) charged particles (ions and electrons) accelerated by solar flares or interplanetary shocks (Richardson 2004). SEPs are known to cause heating, ionization and chemical changes in terrestrial planet atmospheres (Seppälä et al. 2008) and have been observed to cause ionization in the Martian atmosphere (Lillis et al. 2012; Morgan et al. 2006; Sánchez-Cano et al. 2019), as well as auroral emission (Schneider et al. 2015). Their effects are typically unevenly distributed across Mars due to their directional anisotropy (Lillis et al. 2016) and (particularly for electrons) sensitivity to Mars' crustal magnetic fields. Whether the effects of SEPs alone cause increases in the escape rate of planetary ions from Mars is still unclear-but as part of the larger space weather effects question they are of major interest to the broader problem of Mars climate evolution (Futaana et al. 2008). Both flares and SEP events are thought to have been stronger and/or more frequent in the early solar system (Lillis et al. 2015; Walker 1975). Studying this behavior will further shed light on the connection between the lower atmospheric events and the thermal and photochemical escape rates from the Martian atmosphere.

EMUS will observe the response of the Martian thermosphere, exosphere, and neutral escape rates to SEP events, as well as possibly the auroral emission from SEP events. Our primary information source for the timing and intensity of SEP events will be the MAVEN Solar Energetic Particle detector, which provides energy spectra of energetic electrons (20 keV–1 MeV) and ions (20 keV–12 MeV) at a variable cadence not less than once per minute (Larson et al. 2015). We will augment this information with energetic particle backgrounds from EMUS itself, which are mainly caused by >20 MeV protons (e.g. Delory et al. 2012).

The strategy for this analysis is to study the effect of SEP events and CMEs on escape rates using in-situ space weather data from Mars. However, if such data are not available, the WSA-ENLIL (Odstrcil 2003) model can be used in their place (see Fig. 9). The ENLIL model assists in predicting the propagation of CMEs through the heliosphere based on solar observations. This will help in understanding the effects of CMEs on the planet and how they may play an important role in the upper atmosphere conditions and on ionospheric dynamics (Luhmann et al. 2017). In addition, the LMD-MGCM will be used to provide theoretical expectations on the impact of SEPs and CMEs on the thermosphere of Mars.

5.3.4 B3.4: Polar Cap Variability

Martian polar ice caps consist of mostly carbon dioxide and water ice. The ice caps grow during the fall and winter as gas from the atmosphere freezes onto the surface and then sublimate during the spring and summer as the ice on the surface goes back into the atmosphere (for a review, see Titus et al. 2017). The polar region is covered by CO_2 ice if the surface temperature is ~ 145 K. Warmer surfaces up to ~ 190 K may have H_2O ice, while surfaces that are warmer yet are bare ground as shown in Fig. 10 (Forget 2009). Studies using (for example) Viking Orbiter and Mars Global Surveyor observations have tracked the variable extent and albedo variations of the polar caps (Bass and Paige 2000; Benson and James 2005; Titus 2005) and a strong correlation between the presence of surface ice and atmospheric water vapor has been observed (Pankine et al. 2009; Khayat et al. 2019). We plan to monitor the atmospheric changes in response to polar cap variability to work on understanding the connection, if any, between it and atmospheric escape.

Fig. 9 WSA-ENLIL simulations provided by the Space Weather Prediction Center will provide heliospheric context for space weather impacts on the Mars upper atmosphere that EMM will investigate

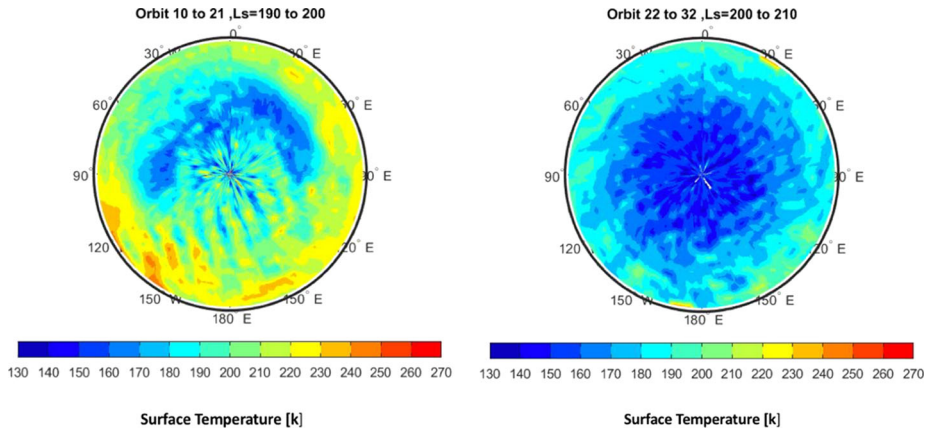
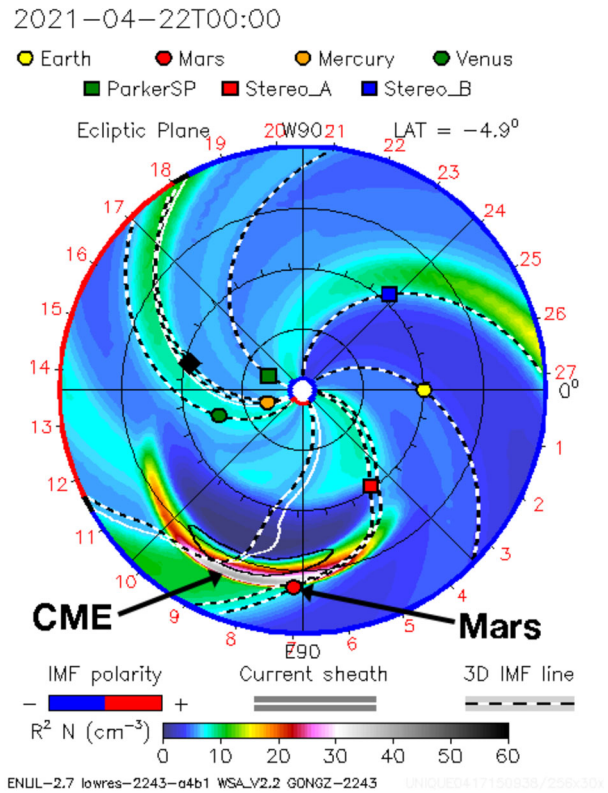


Fig. 10 South polar cap mapping for the observations in orbits 10-32 ($L_s=190^{\circ}$ – 210°) using TES aerobraking data. The right panel shows night time observation while the left panel shows daytime observation

EMIRS surface temperature data and EXI visible images will be used to study polar cap surface temperature and albedo variation on a sub-seasonal timescale. EMIRS determines the surface temperature of Mars by calculating the brightness temperature at wavenumber 1300 cm^{-1} , where the atmosphere of Mars is almost transparent and the radiance is not

absorbed by the atmospheric gases and aerosols. The LMD-MGCM will also provide the theoretical expectations needed for polar cap spatial and temporal variability.

5.3.5 B3.5: Dust Deposition and Removal Events

The global distribution and mobility of dust is a key factor in both Martian geology and climate interpretations. The Martian dust is perhaps the strongest control on the Martian climate, dramatically impacting atmospheric conditions. The deposition and removal of dust have an effect on Mars surface temperatures (daytime and nighttime) and albedo (Szwast et al. 2006; Cantor 2007; Smith 2004). We plan to monitor the events of dust deposition and removal to enhance our understanding of the Martian atmosphere dynamics. EMM will retrieve the dust column integrated optical depth using EMIRS observed spectra to determine the geographic and diurnal variation of dust optical depth on sub-seasonal timescales, with accuracy of $\pm 5\%$ with a spatial resolution of 100–300 km diameter pixels. EMIRS surface temperature data and EXI visible images from the red band will be used to measure surface temperature over the full diurnal cycle and capture albedo variations on a seasonal timescale. Analysis of this data will allow estimates of deposition and removal of dust and how it affects the surface temperature and albedo of Mars. The KRC thermal model in JAMRS will be used to compute diurnal temperatures on Mars over the full seasonal range; the KRC thermal model uses thermal wavelengths to determine the radiative effect of a dusty atmosphere and compute globally the annual average surface temperature and albedo (Kieffer 2013).

6 Objective C: Characterize the Spatial Structure and Variability of Key Constituents in the Martian Exosphere

EMM Objective C focuses on characterizing the spatial structure and variability of the Martian exosphere, the collisionless upper region of the atmosphere where escape to space can be most directly characterized. Specifically, the EMUS instrument measures hydrogen and oxygen through observations of solar resonant fluorescence that are then converted from brightnesses to geophysical densities as part of the EMUS data processing. Objective C is fulfilled through analysis of these density data products, producing new information on the processes that govern exospheric dynamics and escape. We identified three key analyses, described in the following sections, to be performed in achieving this objective: (C1) comparing the EMUS derived density structures to model predictions; (C2) deriving hydrogen and oxygen escape rates and variability from derived density profiles; and (C3) comparing EMUS derived escape rates to model predictions. Table 3 summarizes required data, physical models and tools for each analysis.

6.1 C1: Comparison of EMUS Derived Densities with Model Predictions

The Hope Probe will perform raster scans imaging the Martian inner corona and will slew out to ± 50 degrees in an asterisk pattern to provide EMUS observations with the first 3D picture of hydrogen densities in terms of longitudes, latitudes and altitudes (Holsclaw et al. 2021). EMM's frequent observations of the exosphere from all phase angles will be sensitive to anisotropy in the atmosphere, enabling detailed studies of exospheric dynamics and hydrogen escape.

Based on MAVEN data analyses and developed models, it is predicted that hydrogen and oxygen densities will be greatly impacted by seasonal and spatial variabilities (Lillis et al.

Table 3 Mapping of objective C analyses to needed EMM data, and other data, tools, and physical models

Objective C Analyses:		(C1)	(C2)	(C3)
<i>EMM Data</i>				
EMIRS	Atmospheric and surface temperatures			
	Dust optical depth at 9 μm			
	Water vapor column abundance at 25-40 μm			
	Ice optical depth at 12 μm			
EXI	Ice optical depth at 320 nm			
	Ozone column abundance at 260 nm			
	Visible image of Mars			
EMUS	Thermospheric oxygen and carbon monoxide column			
	Density of hydrogen and oxygen corona	*	*	
<i>Others (related to objective C)</i>				
Data	EMUS derived escape rates			*
Tools	JMARS Visualization			
Models	LMD-MGCM	*		*
	Additional H atom microphysical models		*	
	3D Oxygen Photochemical escape model		*	
	3D Hydrogen Jeans Escape Model		*	

2015; Chaffin et al. 2015; Chaufray et al. 2015; Lee et al. 2015, 2018). There are many factors that can lead to these variabilities, from temperature differences driven by solar activity or change of seasons, to thermospheric winds and local time effects. To thoroughly interpret EMUS datasets, it is vital to compare them with outputs from numerical atmospheric models to understand these variations. For example, running various eddy diffusion coefficients through numerical models to analyze how they affect hydrogen distribution in the thermosphere and exosphere, then matching them with EMUS datasets to pinpoint the eddy diffusion rate from real data—ultimately providing us with new knowledge of the Martian atmosphere's physics. The focus of this analysis is to identify key parameters that we predict will drive spatial and temporal variability to EMUS observed constituents and then testing them through numerical models. This will help us recognize the magnitude and span in which these parameters have an effect on EMUS observed quantities and their variations. Moreover, these numerical models will be utilized as comparison and verification tools for EMUS retrievals.

This analysis will rely on EMUS data products, specifically the exospheric hydrogen (Lyman alpha, 121.6 nm & Lyman beta 102.6 nm) and exospheric oxygen densities (130.4 nm) as a function of longitude, latitude and altitude around Mars. The model used for this analysis will be the LMD-GCM, which incorporates thermosphere and exosphere dynamics, simulating the 3D distribution of both hydrogen and oxygen.

6.2 C2: Derivation of Hydrogen and Oxygen Escape Rates and Variability from Derived Density Profiles

Water escape from Mars over geologic time is one of the contributing factors to the global transformation of the Martian atmosphere from a wetter atmosphere to a dryer atmosphere.

Hydrogen and oxygen, the components of water, are the key constituents forming the Martian exosphere and their escape to space are the most significant. Both charged and uncharged atomic and molecular hydrogen and oxygen escape Mars leading to both ion escape and neutral escape. EMM will focus on studying and deriving the latter sub-seasonally from oxygen and hydrogen densities and altitude profiles, measured by EMUS instrument, as escape rates differ with season and solar activity in a non-steady fashion (Rahmati et al. 2018).

Neutral atoms escape Mars when they reach escape energy sufficient to escape the gravitational force of Mars. Those that do not gain enough energy become gravitationally bound to Mars forming the corona around it. Escape energies differ based on species and are primarily gained by Jeans, photochemical or sputtering processes. Hydrogen is the lightest species, thus having the lowest escape energy, while oxygen comparably is heavier and has a greater escape energy (Chaufray et al. 2007). Hydrogen also escapes Mars through the Jeans escape process, while escaping oxygen is primarily generated via photochemical processes.

6.2.1 Hydrogen Escape

Exospheric hydrogen is ultimately sourced from water vapor lower in the atmosphere, either via the 'classical' paradigm whereby molecular hydrogen is formed from water throughout the bottom several scale heights of the atmosphere before being transported upward, where it is dissociated into thermospheric atomic hydrogen (e.g. McElroy 1972a; Parkinson and Hunten 1972), or via much more direct transport of water to middle or upper atmospheric altitudes where it can produce atomic H, as has been indicated in many recent studies (e.g. Chaffin et al. 2014; Clarke et al. 2014; Stone et al. 2020). Once present in the upper thermosphere, hydrogen atoms in the high-energy tail of the Maxwell-Boltzmann distribution form the nearly collisionless H corona, which includes a small but important component of escaping atoms.

6.2.2 Oxygen Escape

Exospheric oxygen above ~ 700 km is primarily non-thermal and produced by dissociative recombination of molecular oxygen ions (O_2^+) in the ionosphere, with peak ion concentrations occurring in the lower thermosphere of Mars (Hanson et al. 1976; Fox and Hać 2009). This exothermic reaction results in fast neutral oxygen atoms which are transported from the collisional atmosphere to the near-collisionless exosphere of Mars where they form the oxygen corona. The energy gained from the dissociative recombination process is dependent on electrons' relative velocities and O_2^+ electron and ion temperature. A fraction of this population has velocities exceeding the Martian escape velocity, and can be lost to space from the base of the exosphere if they do not have too many collisions with the thermal background gas.

6.2.3 Strategy for Escape Rate Calculations

Calculating hydrogen Jeans escape rate and oxygen photochemical escape rate depends on hydrogen and oxygen densities and temperatures in the upper atmosphere, along with atomic transport models. The densities are very dependent on the dynamics of the lower atmosphere, where water sublimates, and they vary widely geographically and seasonally. The temperatures are also dependent on the lower atmosphere heating, in addition to the solar EUV heating.

EMM will derive hydrogen escape using measurements from both optically thick H I 121.6 nm Lyman alpha emission and optically thin H I 102.6 nm Lyman beta emission close to the planet. While periodic measurements of H Lyman beta up to 6 Mars radii reduces the model-dependency in the escape derivation, the measurement of H Lyman alpha up to 10 Mars radii (where it becomes optically thin) enables the separation of hot escaping hydrogen from the cold bounded hydrogen. Hydrogen column densities will be derived directly from H Lyman beta intensities measured up to 6 Mars radii, thus constraining the three-dimensional representation of the exosphere. Altitude profiles of hydrogen in the exosphere will be used in a Jeans escape model (Clarke et al. 2014; Chaffin et al. 2014, 2018) that computes density structure of the atmosphere and escape rates from density and temperature at the exobase assuming Maxwellian velocity distributions. Additional H atom microphysical models with appropriate collision cross sections and chemistry as LMD-MGCM will be used to compute a priori escape rates from assumptions about the atmosphere.

EMM will also derive oxygen escape using measurements from O I 130.4 nm at altitudes where it is optically thin. Periodic measurements from 1.06 up to 6 Mars radii, will enable the distinction of escaping oxygen from gravitationally bound oxygen. Altitude profiles of O in the exosphere will be used in a hot oxygen exosphere model (Deighan et al. 2015) that computes oxygen density profile and escape rates from known or assumed chemical reaction rates and collision cross sections will be used.

Uncertainties from deriving hydrogen and oxygen escape rates using the physical escape models will be determined. Also, simpler analytic models will be employed inverting coronal profiles to obtain velocity distributions at the exobase, assuming spherical symmetry and a collision-less exosphere. Extrapolations of these analytically derived velocity distributions can then be used to derive escape rates and compared to more detailed model predictions.

6.3 C3: Comparison of Derived Escape Rates to Model Predictions

This analysis focuses on comparing the derived escape rates from EMUS data, in Sect. 6.2, to escape rates generated from model predictions. The need for this analysis stems from the absence of some information specific to Mars atmosphere physical state, or specific to EMUS observation parameters (e.g. location, season) at the time of EMM data retrieval. The comparison will reveal the ability of current models in deriving escape rates as seen on Mars today. Differences between escape rates will indicate missing physical processes in the models or will bring new information on current Mars atmosphere processes. Also, it will help in answering the stoichiometric escape question on whether hydrogen and oxygen escape in the 2:1 ratio present in the water molecule (McElroy and Donahue 1972b; Jakosky et al. 2017).

This analysis will utilize the LMD-MGCM and 1D photochemical codes as prior models to simulate and predict hydrogen and oxygen escape rates over the course of the mission, to then be compared to rates derived from EMM data. Utilizing a model library with a wide parameter space is expected to be necessary to accurately capture Martian atmospheric physics, and to investigate the effect of episodic events, Sect. 5.3, on escape rates, especially with respect to solar or astronomical events.

7 Conclusion

The EMM/Hope probe, arrived at Mars on February 9, 2021 and will study the Martian atmosphere during a primary mission of one Martian year. With its unprecedented orbit,

EMM's observations will reveal atmospheric behavior and connections to form a new and global perspective. Here, we summarized and identified the strategy put forward by the EMM science team to achieve the scientific goals and objectives set for the mission. The basic strategy utilizes EMM data, including its unique combination of temporal and spatial coverage, to test our current understanding of Martian atmosphere, including that obtained from global circulation models and previous scientific missions to Mars. The strategy can be adapted to any unanticipated changes in instrument or spacecraft performance as the science phase data arrives from the EMIRS, EXI, and EMUS scientific instruments. In addition, the tools and models will be updated based on the analyses of the observations. EMM measurements will provide a significantly improved understanding of circulation and weather in the Martian atmosphere while revealing the mechanisms behind the upward transport of energy and particles and the subsequent escape of atmospheric constituents from the gravity of Mars. The mission's unique combination of instrumental synergy and temporal and spatial coverage of Mars' different atmospheric layers will open a new and much-needed window into the workings of the atmosphere of our planetary neighbor.

Acknowledgements We thank Jeffrey S. Parker from Advanced Space for supporting this work by providing information related to EMM orbital parameters and geographical and diurnal coverage.

Funding Funding for development of the EMM mission was provided by the UAE government, and to co-authors outside of the UAE by MBRSC.

Declarations

Compliance with Ethical Standards The authors have complied with the ethical standards of Space Science Reviews in preparing this manuscript and conducting any analysis described therein.

Conflict of Interest The authors declare that they have no conflict of interest.

Ethical approval The authors approve the ethical standards declaration above.

Informed consent All authors have been informed of and agreed to the submission of this manuscript.

Open Access This article is licensed under a Creative Commons Attribution 4.0 International License, which permits use, sharing, adaptation, distribution and reproduction in any medium or format, as long as you give appropriate credit to the original author(s) and the source, provide a link to the Creative Commons licence, and indicate if changes were made. The images or other third party material in this article are included in the article's Creative Commons licence, unless indicated otherwise in a credit line to the material. If material is not included in the article's Creative Commons licence and your intended use is not permitted by statutory regulation or exceeds the permitted use, you will need to obtain permission directly from the copyright holder. To view a copy of this licence, visit <http://creativecommons.org/licenses/by/4.0/>.

References

- S. Amiri, D. Brain, O. Sharaf, P. Withnell, M. McGrath, B. Landin, B. Pramann, B. Harter, C. Sanders, C. Edwards, D. Kubitschek, E. Pilinski, G. Holsclaw, H. Reed, H. Al Matroushi, J. Parker, J. Deighan, M. Kelley, M. Chaffin, M. Packard, M. Smith, M. Al Awadhi, N. Ferrington, O. Al Shehhi, O. Al Hamadi, R. Wrigley, R. Lillis, S. Ryan, S. Al Dhafri, Z. Al Shamsi, A. Jones, B.M. Jakosky, E. Al Tunaiji, F. Lootah, F. Forget, H. Al Mazmi, J. Luhmann, K. Badri, M. Al Shamsi, M. Yousuf, M. Fillingim, M. Wolff, M. Osterloo, N. Al Mheiri, P. Christensen, S. England, S. Jain, *Space Sci. Rev.* (2021), this journal
- M. Angelats i Coll, F. Forget, M.A. López-Valverde, F. González-Galindo, *Geophys. Res. Lett.* **32**, L04201 (2005). <https://doi.org/10.1029/2004GL021368>

- S. Aoki, A.C. Vandaele, F. Daerden, G.L. Villanueva, G. Liuzzi, I.R. Thomas, J.T. Erwin, L. Trompet, S. Robert, L. Neary, S. Viscardy, R.T. Clancy, M.D. Smith, M.A. Lopez-Valverde, B. Hill, B. Ristic, M.R. Patel, G. Bellucci, J.J. Lopez-Moreno, J. Geophys. Res., Planets **124**, 3482 (2019). <https://doi.org/10.1029/2019je006109>
- M.J. Aschwanden, J.-P. Wülsler, N.V. Nitta, J.R. Lemen, S. Freeland, W.T. Thompson, Sol. Phys. **289**, 919 (2014). <https://doi.org/10.1007/s11207-013-0378-5>
- J.R. Barnes, R.M. Haberle, R.J. Wilson, S.R. Lewis, J.R. Murphy, P.L. Read, in *The Atmosphere and Climate of Mars*, ed. by R.M. Haberle, R.T. Clancy, F. Forget, M.D. Smith, R.W. Zurek (Cambridge University Press, Cambridge, 2017)
- D.S. Bass, D.A. Paige, Icarus **144**, 397 (2000). <https://doi.org/10.1006/icar.1999.6301>
- J.L. Benson, P.B. James, Icarus **174**, 513 (2005). <https://doi.org/10.1016/j.icarus.2004.08.025>
- S.W. Bougher, J. Murphy, R. Haberle, Adv. Space Res. **19**, 1255 (1997). [https://doi.org/10.1016/s0273-1177\(97\)00278-0](https://doi.org/10.1016/s0273-1177(97)00278-0)
- S.W. Bougher, G.M. Keating, R.W. Zurek, J.M. Murphy, R.M. Haberle, J. Hollingsworth, R.T. Clancy, Adv. Space Res. **23**, 1887 (1999). [https://doi.org/10.1016/S0273-1177\(99\)00272-0](https://doi.org/10.1016/S0273-1177(99)00272-0)
- S.W. Bougher, T.E. Cravens, J. Grebowsky, J. Luhmann, Space Sci. Rev. **195**, 423 (2015). <https://doi.org/10.1007/s11214-014-0053-7>
- S.W. Bougher, D.A. Brain, J.L. Fox, F. Gonzalez-Galindo, C. Simon-Wedlund, P.G. Withers, in *The Atmosphere and Climate of Mars*, ed. by R.M. Haberle, R.T. Clancy, F. Forget, M.D. Smith, R.W. Zurek (Cambridge University Press, Cambridge, 2017), pp. 433–463
- D.A. Brain, S. Barabash, S.W. Bougher, F. Duru, B. Jakosky, R. Modolo, in *The Atmosphere and Climate of Mars*, ed. by R.M. Haberle, R.T. Clancy, F. Forget, M.D. Smith, R.W. Zurek (Cambridge University Press, Cambridge, 2017), pp. 464–496
- B.A. Cantor, Icarus **186**(1), 60 (2007). <https://doi.org/10.1016/j.icarus.2006.08.019>
- B.A. Cantor, P.B. James, M. Caplinger, M.J. Wolff, J. Geophys. Res., Planets **106**(E10), 23653 (2001). <https://doi.org/10.1029/2000JE001310>
- B.A. Cantor, N.B. Pickett, M.C. Malin, S.W. Lee, M.J. Wolff, M.A. Caplinger, Icarus **321**, 161 (2019). <https://doi.org/10.1016/j.icarus.2018.10.005>
- M.S. Chaffin, J.-Y. Chaufray, I. Stewart, F. Montmessin, N.M. Schneider, J.-L. Bertaux, Geophys. Res. Lett. **41**, 314 (2014). <https://doi.org/10.1002/2013gl058578>
- M.S. Chaffin, J.Y. Chaufray, J. Deighan, N.M. Schneider, W.E. McClintock, A.I.F. Stewart, E. Thiemann, J.T. Clarke, G.M. Holsclaw, S.K. Jain, M.M.J. Crismani, A. Stiepen, F. Montmessin, F.G. Eparvier, P.C. Chamberlain, B.M. Jakosky, Geophys. Res. Lett. **42**, 9001 (2015). <https://doi.org/10.1002/2015GL065287>
- M.S. Chaffin, J.Y. Chaufray, J. Deighan, N.M. Schneider, M. Mayyasi, J.T. Clarke, E. Thiemann, S.K. Jain, M.M.J. Crismani, A. Stiepen, F.G. Eparvier, W.E. McClintock, A.I.F. Stewart, G.M. Holsclaw, F. Montmessin, B.M. Jakosky, J. Geophys. Res., Planets **123**, 2192 (2018). <https://doi.org/10.1029/2018JE005574>
- J.Y. Chaufray, R. Modolo, F. Leblanc, G. Chanteur, R.E. Johnson, J.G. Luhmann, J. Geophys. Res., Planets **112**, 1676 (2007). <https://doi.org/10.1029/2007JE002915>
- J.-Y. Chaufray, F. Gonzalez-Galindo, F. Forget, M.A. Lopez-Valverde, F. Leblanc, R. Modolo, S. Hess, Icarus **245**, 282 (2015). <https://doi.org/10.1016/j.icarus.2014.08.038>
- P.F. Chen, Living Rev. Sol. Phys. **8**, 1 (2011). <https://doi.org/10.12942/lrsp-2011-1>
- P.R. Christensen, J.L. Bandfield, V.E. Hamilton, S.W. Ruff, H.H. Kieffer, T. Titus, M.C. Malin, R.V. Morris, M.D. Lane, R.N. Clark, B.M. Jakosky, M.T. Mellon, J.C. Pearl, B.J. Conrath, M.D. Smith, R.T. Clancy, R.O. Kuzmin, T. Roush, G.L. Mehall, N. Gorelick, K. Bender, K. Murray, S. Dason, E. Greene, S.H. Silverman, M. Greenfield, J. Geophys. Res., Planets **106**, 23823 (2001). <https://doi.org/10.1029/2000JE001370>
- P.R. Christensen, E. Engle, S. Anwar, S. Dickenshied, D. Noss, N. Gorelick, M. Weiss-Malik JMARS—A Planetary GIS (ID: IN22A–06, 2009). <https://ui.adsabs.harvard.edu/abs/2009AGUFMIN22A..06C/abstract>. Accessed 30 May 2020
- R.T. Clancy, A.W. Grossman, M.J. Wolff, P.B. James, D.J. Rudy, Y.N. Billawala, B.J. Sandor, S.W. Lee, D.O. Muhleman, Icarus **122**, 36 (1996). <https://doi.org/10.1006/icar.1996.0108>
- R.T. Clancy, M.J. Wolff, F. Lefèvre, B.A. Cantor, M.C. Malin, M.D. Smith, Icarus **266**, 112 (2016). <https://doi.org/10.1016/j.icarus.2015.11.016>
- R.T. Clancy, F. Montmessin, J. Benson, F. Daerden, A. Colaprete, M.J. Wolff, in *The Atmosphere and Climate of Mars*, ed. by R.M. Haberle, R.T. Clancy, F. Forget, M.D. Smith, R.W. Zurek (Cambridge University Press, Cambridge, 2017), pp. 76–105
- J.T. Clarke, Nat. Astron. **2**, 114 (2018). <https://doi.org/10.1038/s41550-018-0383-6>
- J.T. Clarke, J.-L. Bertaux, J.-Y. Chaufray, G.R. Gladstone, E. Quemerais, J.K. Wilson, D. Bhattacharyya, Geophys. Res. Lett. **41**, 8013 (2014). <https://doi.org/10.1002/2014GL061803>

- S.M. Curry, J.G. Luhmann, Y.J. Ma, C.F. Dong, D. Brain, F. Leblanc, R. Modolo, Y. Dong, J. McFadden, J. Halekas, J. Connerney, J. Espley, T. Hara, Y. Harada, C. Lee, X. Fang, B. Jakosky, *Geophys. Res. Lett.* **42**, 9095 (2015). <https://doi.org/10.1002/2015GL065304>
- D.W. Davies, *J. Geophys. Res.* **84**, 8289 (1979). <https://doi.org/10.1029/jb084ib14p08289>
- J. Deighan, M.S. Chaffin, J.-Y. Chaufray, A.I.F. Stewart, N.M. Schneider, S.K. Jain, A. Stiepen, M. Crismani, W.E. McClintock, J.T. Clarke, G.M. Holsclaw, F. Montmessin, F.G. Eparvier, E.M.B. Thiemann, P.C. Chamberlin, B.M. Jakosky, *Geophys. Res. Lett.* **42**, 9009 (2015). <https://doi.org/10.1002/2015gl065487>
- G.T. Delory, J.G. Luhmann, D. Brain, R.J. Lillis, D.L. Mitchell, R.A. Mewaldt, T.V. Falkenberg, *Space Weather* **10**, S06003 (2012). <https://doi.org/10.1029/2012SW000781>
- S. Dickenshied, P.R. Christensen, S. Carter, S. Anwar, D. Noss, Visualizing Earth and Planetary Remote Sensing Data Using JMARS (ID: IN52A-04, 2014). <https://ui.adsabs.harvard.edu/abs/2014AGUFMIN52A..04D/abstract>. Accessed 30 May 2020
- C.S. Edwards, P.R. Christensen, G.L. Mehall, S. Anwar, E. AlTeneiji, K. Badri, H. Bowles, S. Chase, Z. Farkas, T. Fisher, J. Janiczek, I. Kubik, K. Harris-Laurila, I. Lazbin, E. Madril, M. McAdam, M. Miner, W. O'Donnell, C. Ortiz, D. Pelham, M. Patel, K. Shamordola, T. Tourville, M.D. Smith, N. Smith, R. Woodward, H. Reed, *Space Sci. Rev.* (2021). <https://doi.org/10.1007/s11214-021-00848-1>
- M.K. Elrod, S.M. Curry, E.M.B. Thiemann, S.K. Jain, *Geophys. Res. Lett.* **45**, 8803 (2018). <https://doi.org/10.1029/2018gl077729>
- M.K. Elrod, S.W. Bougher, K. Roeten, R. Sharrar, J. Murphy, *Geophys. Res. Lett.* **47**, e2019GL084378 (2019). <https://doi.org/10.1029/2019GL084378>
- F.G. Eparvier, P.C. Chamberlin, T.N. Woods, E.M.B. Thiemann, *Space Sci. Rev.* **195**, 293 (2015). <https://doi.org/10.1007/s11214-015-0195-2>
- X. Fang, S.W. Bougher, R.E. Johnson, J.G. Luhmann, Y. Ma, Y. Wang, M.W. Liemohn, *Geophys. Res. Lett.* **40**, 1922 (2013). <https://doi.org/10.1002/grl.50415>
- X. Fang, D. Pawlowski, Y. Ma, S. Bougher, E. Thiemann, F. Eparvier, W. Wang, C. Dong, C.O. Lee, Y. Dong, M. Benna, M. Elrod, P. Chamberlin, P. Mahaffy, B. Jakosky, *Geophys. Res. Lett.* **46**, 9334 (2019). <https://doi.org/10.1029/2019GL084515>
- X. Fang, Y. Ma, Y. Lee, S. Bougher, G. Liu, M. Benna, P. Mahaffy, L. Montabone, D. Pawlowski, C. Dong, Y. Dong, B. Jakosky, *J. Geophys. Res. Space Phys.* **125**, e2019JE006111 (2020). <https://doi.org/10.1029/2019JA026838>
- A. Fedorova, J.-L. Bertaux, D. Betsis, F. Montmessin, O. Korabiev, L. Maltagliati, J. Clarke, *Icarus* **300**, 440 (2018). <https://doi.org/10.1016/j.icarus.2017.09.025>
- A.A. Fedorova, F. Montmessin, O. Korabiev, M. Luginin, A. Trokhimovskiy, D.A. Belyaev, N.I. Ignatiev, F. Lefèvre, J. Alday, P.G.J. Irwin, K.S. Olsen, J.-L. Bertaux, E. Millour, A. Määttänen, A. Shakun, A.V. Grigoriev, A. Patrakeev, S. Korsá, N. Kokonkov, L. Baggio, F. Forget, C.F. Wilson, *Science* **367**, 297 (2020). <https://doi.org/10.1126/science.aay9522>
- M. Felici, P. Withers, M.D. Smith, F. González-Galindo, K. Oudrhiri, D. Kahan, *J. Geophys. Res. Space Phys.* **125**, e2019JA027083 (2020). <https://doi.org/10.1029/2019JA027083>
- L. Fletcher, B.R. Dennis, H.S. Hudson, S. Krucker, K. Phillips, A. Veronig, M. Battaglia, L. Bone, A. Caspi, Q. Chen, P. Gallagher, P.T. Grigis, H. Ji, W. Liu, R.O. Milligan, M. Temmer, *Space Sci. Rev.* **159**, 19 (2011). <https://doi.org/10.1007/s11214-010-9701-8>
- F. Forget, *Eur. Phys. J. Conf.* **1**, 235 (2009). <https://doi.org/10.1140/epjconf/e2009-0924-9>
- F. Forget, F. Hourdin, R. Fournier, C. Hourdin, O. Talagrand, M. Collins, S.R. Lewis, P.L. Read, J.-P. Huot, *J. Geophys. Res., Planets* **104**, 24155 (1999). <https://doi.org/10.1029/1999JE001025>
- J.L. Fox, A.B. Hač, *Icarus* **204**, 527 (2009). <https://doi.org/10.1016/j.icarus.2009.07.005>
- Y. Futaana, S. Barabash, M. Yamauchi, S. McKenna-Lawlor, R. Lundin, J.G. Luhmann, D. Brain, E. Carlsson, J.-A. Sauvaud, J.D. Winningham, R.A. Frahm, P. Wurz, M. Holmström, H. Gunell, E. Kallio, W. Baumjohann, H. Lammer, J.R. Sharber, K.C. Hsieh, H. Andersson, A. Grigoriev, K. Brinkfeldt, H. Nilsson, K. Asamura, T.L. Zhang, A.J. Coates, D.R. Linder, D.O. Kataria, C.C. Curtis, B.R. Sandel, A. Fedorov, C. Mazelle, J.-J. Thocaven, M. Grande, H.E.J. Koskinen, T. Sales, W. Schmidt, P. Riihela, J. Kozyra, N. Krupp, J. Woch, M. Fränz, E. Dubinin, S. Orsini, R. Cerulli-Irelli, A. Mura, A. Milillo, M. Maggi, E. Roelof, P. Brandt, K. Szego, J. Scherrer, P. Bochsler, *Planet. Space Sci.* **56**, 873 (2008). <https://doi.org/10.1016/j.pss.2007.10.014>
- P.J. Gierasch, R.M. Goody, *J. Atmos. Sci.* **29**, 400 (1972)
- F. González-Galindo, F. Forget, M.A. López-Valverde, M. Angelats i Coll, E. Millour, *J. Geophys. Res., Planets* **114**, 91 (2009). <https://doi.org/10.1029/2008JE003246>
- F. González-Galindo, J.-Y. Chaufray, M.A. López-Valverde, G. Gilli, F. Forget, F. Leblanc, R. Modolo, S. Hess, M. Yagi, *J. Geophys. Res., Planets* **118**, 2105 (2013). <https://doi.org/10.1002/jgre.20150>
- S.D. Guzewich, M.D. Smith, *J. Geophys. Res., Planets* **124**, 636 (2019). <https://doi.org/10.1029/2018JE005843>

- R.M. Haberle, R. Todd Clancy, F. Forget, M.D. Smith, R.W. Zurek, *The Atmosphere and Climate of Mars* (Cambridge University Press, Cambridge, 2017)
- J.S. Halekas, *J. Geophys. Res., Planets* **122**, 901 (2017). <https://doi.org/10.1002/2017JE005306>
- W.B. Hanson, S. Sanatani, D. Zuccaro, Retarding potential analyzer measurements from Viking Landers. *Trans. Am. Geophys. Union* **57**, 966 (1976)
- N.G. Heavens, D.J. McCleese, M.I. Richardson, D.M. Kass, A. Kleinböhl, J.T. Schofield, *J. Geophys. Res., Planets* **116**, 801 (2011). <https://doi.org/10.1029/2010JE003677>
- N.G. Heavens, A. Kleinböhl, M.S. Chaffin, J.S. Halekas, D.M. Kass, P.O. Hayne, D.J. McCleese, S. Piqueux, J.H. Shirley, J.T. Schofield, *Nat. Astron.* **2**, 126 (2018). <https://doi.org/10.1038/s41550-017-0353-4>
- G. Holsclaw, J. Deighan, H. Almatroushi, M. Chaffin, J. Correia, J.S. Evans, M. Fillingim, A. Hoskins, R. Lillis, F. Lootah, J. McPhate, O. Siegmund, R. Soufli, K. Tyagi, *Space Sci. Rev.* (2021). <https://doi.org/10.1007/s11214-021-00854-3>
- M.N. Izakov, O.P. Krasicki, Effect of nonthermal escape of atoms on Martian atmosphere composition. *Trans. Am. Geophys. Union* **58**, 749 (1977)
- S.K. Jain, J. Deighan, N.M. Schneider, A.I.F. Stewart, J.S. Evans, E.M.B. Thiemann, M.S. Chaffin, M. Crismani, M.H. Stevens, M.K. Elrod, A. Stiepen, W.E. McClintock, D.Y. Lo, J.T. Clarke, F.G. Eparvier, F. Lefèvre, F. Montmessin, G.M. Holsclaw, P.C. Chamberlin, B.M. Jakosky, *Geophys. Res. Lett.* **45**, 7312 (2018). <https://doi.org/10.1029/2018gl077731>
- S.K. Jain, S.W. Bougher, J. Deighan, N.M. Schneider, F. González Galindo, A.I.F. Stewart, R. Sharrar, D. Kass, J. Murphy, D. Pawlowski, *Geophys. Res. Lett.* **47**, e2019GL085302 (2020). <https://doi.org/10.1029/2019GL085302>
- B.M. Jakosky, MAVEN Project Status and Science Highlights, in *38th Mars Exploration Program Analysis Group Meeting, Virtual*, (2020). https://mepag.jpl.nasa.gov/meeting/2020-04/Day3/13_Jakosky-maven-mepag-april-2020-v3_post.pdf. Accessed 14 September 2020
- B.M. Jakosky, C.B. Farmer, *J. Geophys. Res., Solid Earth* **87**, 2999 (1982). <https://doi.org/10.1029/jb087ib04p02999>
- B.M. Jakosky, M. Chaffin, J. Deighan, D. Brain, J.S. Halekas, Are H and O Being Lost from the Mars Atmosphere in the H₂O Stoichiometric Ratio of 2:1? in *American Geophysical Union Fall Meeting*, (2017). <https://ui.adsabs.harvard.edu/abs/2017AGUFM.P34B..02J/abstract>. Accessed 30 May 2020
- B.M. Jakosky, D. Brain, M. Chaffin, S. Curry, J. Deighan, J. Grebowsky, J. Halekas, F. Leblanc, R. Lillis, J.G. Luhmann, L. Andersson, N. Andre, D. Andrews, D. Baird, D. Baker, J. Bell, M. Benna, D. Bhattacharyya, S. Bougher, C. Bowers, P. Chamberlin, J.-Y. Chaufray, J. Clarke, G. Collinson, M. Combi, J. Connerney, K. Connour, J. Correia, K. Crabb, F. Crary, T. Cravens, M. Crismani, G. Delory, R. Dewey, G. DiBraccio, C. Dong, Y. Dong, P. Dunn, H. Egan, M. Elrod, S. England, F. Eparvier, R. Ergun, A. Eriksson, T. Esmann, J. Easley, S. Evans, K. Fallows, X. Fang, M. Fillingim, C. Flynn, A. Fogle, C. Fowler, J. Fox, M. Fujimoto, P. Garnier, Z. Girazian, H. Groeller, J. Gruesbeck, O. Hamil, K.G. Hanley, T. Hara, Y. Harada, J. Hermann, M. Holmberg, G. Holsclaw, S. Houston, S. Inui, S. Jain, R. Jolitz, A. Kotova, T. Kuroda, D. Larson, Y. Lee, C. Lee, F. Lefevre, C. Lentz, D. Lo, R. Lugo, Y.-J. Ma, P. Mahaffy, M.L. Marquette, Y. Matsumoto, M. Mayyasi, C. Mazelle, W. McClintock, J. McFadden, A. Medvedev, M. Mendillo, K. Meziane, Z. Milby, D. Mitchell, R. Modolo, F. Montmessin, A. Nagy, H. Nakagawa, C. Narvaez, K. Olsen, D. Pawlowski, W. Peterson, A. Rahmati, K. Roeten, N. Romanelli, S. Ruhunusiri, C. Russell, S. Sakai, N. Schneider, K. Seki, R. Sharrar, S. Shaver, D.E. Siskind, M. Slipiski, Y. Soobiah, M. Steckiewicz, M.H. Stevens, I. Stewart, A. Stiepen, S. Stone, V. Tenishev, N. Terada, K. Terada, E. Thiemann, R. Tolson, G. Toth, J. Trovato, M. Vogt, T. Weber, P. Withers, S. Xu, R. Yelle, E. Yigit, R. Zurek, *Icarus* **315**, 146 (2018). <https://doi.org/10.1016/j.icarus.2018.05.030>
- A.R. Jones, M. Wolff, M. Alshamsi, M. Osterloo, P. Bay, S. Bramer, N. Brennan, K. Bryant, Z. Castleman, A. Curtin, E. DeVito, V.A. Drake, D. Ebuén, J. Espejo, J. Farren, B. Fenton, C. Fisher, M. Fisher, K. Fortier, S. Gerwig, B. Heberlein, C. Jeppesen, M.A. Khoory, S. Knappmiller, J. Knavel, K. Koski, K. Looney, P. Lujan, M. Miller, G. Newcomb, G. Otzinger, H. Passe, E. Pilinski, H. Reed, R. Shuping, P. Sicken, D. Summers, W. Tighe, S. Wade, L. Walton, J.L. Yaptengco, *Space Sci. Rev.* (2021). <https://doi.org/10.1007/s11214-021-00852-5>
- M.A. Kahre, J.R. Murphy, C.E. Newman, R.J. Wilson, B.A. Cantor, M.T. Lemmon, M.J. Wolff, in *The Atmosphere and Climate of Mars*, ed. by R.M. Haberle, R.T. Clancy, F. Forget, M.D. Smith, R.W. Zurek (Cambridge University Press, Cambridge, 2017), pp. 295–337
- D.M. Kass, A. Kleinböhl, D.J. McCleese, J.T. Schofield, M.D. Smith, *Geophys. Res. Lett.* **43**, 6111 (2016). <https://doi.org/10.1002/2016GL068978>
- G.M. Keating, S.W. Bougher, R.W. Zurek, R.H. Tolson, G.J. Cancro, S.N. Noll, J.S. Parker, T.J. Schellenberg, R.W. Shane, B.L. Wilkerson, J.R. Murphy, J.L. Hollingsworth, R.M. Haberle, M. Joshi, J.C. Pearl, B.J. Conrath, M.D. Smith, R.T. Clancy, R.C. Blanchard, R.G. Wilmoth, D.F. Rault, T.Z. Martin, D.T. Lyons, P.B. Esposito, M.D. Johnston, C.W. Whetzel, C.G. Justus, J.M. Babcic, *Science* **279**, 1672 (1998). <https://doi.org/10.1126/science.279.5357.1672>

- A.S. Khayat, M.D. Smith, S.D. Guzewich, *Icarus* **321**, 722 (2019). <https://doi.org/10.1016/j.icarus.2018.12.024>
- H.H. Kieffer, *J. Geophys. Res., Planets* **118**, 451 (2013). <https://doi.org/10.1029/2012JE004164>
- A. Kleinböhl, R.J. Wilson, D. Kass, J.T. Schofield, D.J. McCleese, *Geophys. Res. Lett.* **40**, 1952 (2013). <https://doi.org/10.1002/grl.50497>
- S. Krucker, G.J. Hurford, Y. Su, W.-Q. Gan, *Res. Astron. Astrophys.* **19**, 167 (2019). <https://doi.org/10.1088/1674-4527/19/11/167>
- D.E. Larson, R.J. Lillis, C.O. Lee, P.A. Dunn, K. Hatch, M. Robinson, D. Glaser, J. Chen, D. Curtis, C. Tiu, R.P. Lin, J.G. Luhmann, B.M. Jakosky, *Space Sci. Rev.* **195**, 153 (2015). <https://doi.org/10.1007/s11214-015-0218-z>
- Y. Lee, M.R. Combi, V. Tennishev, S.W. Bougher, R.J. Lillis, *J. Geophys. Res., Planets* **120**, 1880 (2015). <https://doi.org/10.1002/2015JE004890>
- Y. Lee, C. Dong, D. Pawlowski, E. Thiemann, V. Tennishev, P. Mahaffy, M. Benna, M. Combi, S. Bougher, F. Eparvier, *Geophys. Res. Lett.* **45**, 6814 (2018). <https://doi.org/10.1029/2018GL077732>
- J.R. Lemen, A.M. Title, D.J. Akin, P.F. Boerner, C. Chou, J.F. Drake, D.W. Duncan, C.G. Edwards, F.M. Friedlaender, G.F. Heyman, N.E. Hurlburt, N.L. Katz, G.D. Kushner, M. Levay, R.W. Lindgren, D.P. Mathur, E.L. McFeaters, S. Mitchell, R.A. Rehse, C.J. Schrijver, L.A. Springer, R.A. Stern, T.D. Tarbell, J.-P. Wuelser, C.J. Wolfson, C. Yanari, J.A. Bookbinder, P.N. Cheimets, D. Caldwell, E.E. Deluca, R. Gates, L. Golub, S. Park, W.A. Podgorski, R.I. Bush, P.H. Scherrer, M.A. Gummin, P. Smith, G. Auken, P. Jerram, P. Pool, R. Soufli, D.L. Windt, S. Beardsley, M. Clapp, J. Lang, N. Waltham, *Sol. Phys.* **275**, 17 (2012). <https://doi.org/10.1007/s11207-011-9776-8>
- C.E. Leovy, R.W. Zurek, J.B. Pollack, *J. Atmos. Sci.* **30**(5), 749 (1973)
- S.R. Lewis, P.L. Read, M. Collins, *Planet. Space Sci.* **44**, 1395 (1996). [https://doi.org/10.1016/S0032-0633\(96\)00058-X](https://doi.org/10.1016/S0032-0633(96)00058-X)
- R.J. Lillis, D.A. Brain, G.T. Delory, D.L. Mitchell, J.G. Luhmann, R.P. Lin, *J. Geophys. Res., Planets* **117**, E03004 (2012). <https://doi.org/10.1029/2011je003932>
- R.J. Lillis, D.A. Brain, S.W. Bougher, F. Leblanc, J.G. Luhmann, B.M. Jakosky, R. Modolo, J. Fox, J. Deighan, X. Fang, Y.C. Wang, Y. Lee, C. Dong, Y. Ma, T. Cravens, L. Andersson, S.M. Curry, N. Schneider, M. Combi, I. Stewart, J. Clarke, J. Grebowsky, D.L. Mitchell, R. Yelle, A.F. Nagy, D. Baker, R.P. Lin, *Space Sci. Rev.* **195**, 357 (2015). <https://doi.org/10.1007/s11214-015-0165-8>
- R.J. Lillis, C.O. Lee, D. Larson, J.G. Luhmann, J.S. Halekas, J.E.P. Connerney, B.M. Jakosky, *J. Geophys. Res. Space Phys.* **121**, 2818 (2016). <https://doi.org/10.1002/2015ja022327>
- J.G. Luhmann, M.L. Mays, D. Odstrcil, Y. Li, H. Bain, C.O. Lee, A.B. Galvin, R.A. Mewaldt, C.M.S. Cohen, R.A. Leske, D. Larson, Y. Futaana, *Space Weather* **15**, 934 (2017). <https://doi.org/10.1002/2017SW001617>
- J.-B. Madeleine, F. Forget, E. Millour, L. Montabone, M.J. Wolff, *J. Geophys. Res., Planets* **116**, E11006 (2011). <https://doi.org/10.1029/2011JE003855>
- J.-B. Madeleine, F. Forget, E. Millour, T. Navarro, A. Spiga, *Geophys. Res. Lett.* **39**, L23202 (2012). <https://doi.org/10.1029/2012gl053564>
- M.C. Malin, K.S. Edgett, B.A. Cantor, M.A. Caplinger, G.E. Danielson, E.H. Jensen, M.A. Ravine, J.L. Sandoval, K.D. Supilver, *Mars J.* **5**, 1 (2010). <https://doi.org/10.1555/mars.2010.0001>
- L. Maltagliati, F. Montmessin, A. Fedorova, O. Korabiev, F. Forget, J.-L. Bertaux, *Science* **333**, 1868 (2011). <https://doi.org/10.1126/science.1207957>
- L. Martin, *Icarus* **23**, 108 (1974). [https://doi.org/10.1016/0019-1035\(74\)90108-0](https://doi.org/10.1016/0019-1035(74)90108-0)
- G.M. Martínez, C.N. Newman, A. De Vicente-Retortillo, E. Fischer, N.O. Renno, M.I. Richardson, A.G. Fairén, M. Genzer, S.D. Guzewich, R.M. Haberle, A.-M. Harri, O. Kempainen, M.T. Lemmon, M.D. Smith, M. de la Torre-Juárez, A.R. Vasavada, *Space Sci. Rev.* **212**, 295 (2017). <https://doi.org/10.1007/s11214-017-0360-x#Fig5>
- M. Mayyasi, D. Bhattacharyya, J. Clarke, A. Catalano, M. Benna, P. Mahaffy, E. Thiemann, C.O. Lee, J. Deighan, S. Jain, M. Chaffin, M. Crismani, W. McClintock, I. Stewart, G. Holsclaw, A. Stiepen, F. Montmessin, N. Schneider, B. Jakosky, *Geophys. Res. Lett.* **45**, 8844 (2018). <https://doi.org/10.1029/2018GL077727>
- M.B. McElroy, *Science* **175**, 443 (1972a). <https://doi.org/10.1126/science.175.4020.443>
- M.B. McElroy, T.M. Donahue, *Science* **177**, 986 (1972b). <https://doi.org/10.1126/science.177.4053.986>
- E. Millour, F. Forget, User Manual for the LMD Martian Atmospheric General Circulation Model. Le Laboratoire de Météorologie Dynamique (LMD) (2018). https://www.lmd.jussieu.fr/~lmdz/planets/mars/user_manual.pdf
- L. Montabone, S.R. Lewis, P.L. Read, *Adv. Space Res.* **36**, 2146 (2005). <https://doi.org/10.1016/j.asr.2005.07.047>
- L. Montabone, F. Forget, E. Millour, R.J. Wilson, S.R. Lewis, B. Cantor, D. Kass, A. Kleinböhl, M.T. Lemmon, M.D., Smith, M.J. Wolff, *Icarus* **251**, 65 (2015). <https://doi.org/10.1016/j.icarus.2014.12.034>

- F. Montmessin, M.D. Smith, Y. Langevin, M.T. Mellon, A. Fedorova, in *The Atmosphere and Climate of Mars*, ed. by R.M. Haberle, R.T. Clancy, F. Forget, M.D. Smith, R.W. Zurek (Cambridge University Press, Cambridge, 2017), pp. 338–373
- D.D. Morgan, D.A. Gurnett, D.L. Kirchner, R.L. Huff, D.A. Brain, W.V. Boynton, M.H. Acuña, J.J. Plaut, G. Picardi, *Geophys. Res. Lett.* **33**, 495 (2006). <https://doi.org/10.1029/2006gl026637>
- D. Müller, O.C.St. Cyr, I. Zouganelis, H.R. Gilbert, R. Marsden, T. Nieves-Chinchilla, E. Antonucci, F. Auchère, D. Berghmans, T. Horbury, R.A. Howard, S. Krucker, M. Maksimovic, C.J. Owen, P. Rochus, J. Rodriguez-Pacheco, M. Romoli, S.K. Solanki, R. Bruno, M. Carlsson, A. Fludra, L. Harra, D.M. Hassler, S. Livi, P. Louarn, H. Peter, U. Schühle, L. Teriaca, J.C. del Toro Iniesta, R.F. Wimmer-Schweingruber, E. Marsch, M. Velli, A. De Groof, A. Walsh, D. Williams, *Astron. Astrophys.* **642**, A1 (2020). <https://doi.org/10.1051/0004-6361/202038467>
- T. Navarro, F. Forget, E. Millour, S.J. Greybush, E. Kalnay, T. Miyoshi, *Earth Space Sci.* **4**, 690 (2017). <https://doi.org/10.1002/2017EA000274>
- A.O. Nier, M.B. McElroy, *J. Geophys. Res.* **82**, 4341 (1977). <https://doi.org/10.1029/JS082i028p04341>
- D. Odstrcil, *Adv. Space Res.* **32**, 497 (2003). [https://doi.org/10.1016/S0273-1177\(03\)00332-6](https://doi.org/10.1016/S0273-1177(03)00332-6)
- A.A. Pankine, L.K. Tamppari, M.D. Smith, *Icarus* **204**, 87 (2009). <https://doi.org/10.1016/j.icarus.2009.06.009>
- T.D. Parkinson, D.M. Hunten, *J. Atmos. Sci.* **29**, 1380 (1972). [https://doi.org/10.1175/1520-0469\(1972\)029<1380:SAOOO>2.0.CO;2](https://doi.org/10.1175/1520-0469(1972)029<1380:SAOOO>2.0.CO;2)
- S. Perrier, J.L. Bertaux, F. Lefèvre, S. Lebonnois, O. Korabely, A. Fedorova, F. Montmessin, *J. Geophys. Res., Planets* **111**, 197 (2006). <https://doi.org/10.1029/2006JE002681>
- J.F. Qin, H. Zou, Y.G. Ye, Z.F. Yin, J.S. Wang, E. Nielsen, *J. Geophys. Res., Planets* **124**, 602 (2019). <https://doi.org/10.1029/2018je005864>
- A. Rahmati, D.E. Larson, T.E. Cravens, R.J. Lillis, J.S. Halekas, J.P. McFadden, D.L. Mitchell, E.M.B. Thiemann, J.E.P. Connerney, P.A. Dunn, C.O. Lee, F.G. Eparvier, G.A. DiBraccio, J.R. Espley, J.G. Luhmann, C. Mazelle, B.M. Jakosky, *J. Geophys. Res., Planets* **123**, 1192 (2018). <https://doi.org/10.1029/2018JE005560>
- I.G. Richardson, *Space Sci. Rev.* **111**, 267 (2004). <https://doi.org/10.1023/B:SPAC.0000032689.52830.3e>
- M.I. Richardson, R.J. Wilson, A.V. Rodin, *J. Geophys. Res., Planets* **107**, 4121 (2002). <https://doi.org/10.1029/2001JE001804>
- P. Rochus, F. Auchère, D. Berghmans, L. Harra, W. Schmutz, U. Schühle, P. Addison, T. Appourchaux, R. Aznar Cuadrado, D. Baker, J. Barbay, D. Bates, A. BenMoussa, M. Bergmann, C. Beurthe, B. Borgo, K. Bonte, M. Bouzit, L. Bradley, V. Büchel, E. Buchlin, J. Büchner, F. Cabé, L. Cadiergues, M. Chaigneau, B. Chares, C. Choque Cortez, P. Coker, M. Condamine, S. Coumar, W. Curdt, J. Cutler, D. Davies, G. Davison, J.-M. Defise, G. Del Zanna, F. Delmotte, V. Delouille, L. Dolla, C. Dumesnil, F. Dürig, R. Enge, S. François, J.-J. Fourmond, J.-M. Gillis, B. Giordanengo, S. Gissot, L.M. Green, N. Guerreiro, A. Guilbaud, M. Gyo, M. Haberleiter, A. Hafiz, M. Hailey, J.-P. Halain, J. Hansotte, C. Hecquet, K. Heerlein, M.-L. Hellin, S. Hemsley, A. Hermans, V. Hervier, J.-F. Hochedez, Y. Houbrechts, K. Ihsan, L. Jacques, A. Jérôme, J. Jones, M. Kahle, T. Kennedy, M. Klaproth, M. Kolleck, S. Koller, E. Kotsialos, E. Kraaikamp, P. Langer, A. Lawrenson, J.-C. Le Clech, C. Lenaerts, S. Liebecq, D. Linder, D.M. Long, B. Mampaey, D. Markiewicz-Innes, B. Marquet, E. Marsch, S. Matthews, E. Mazy, A. Mazzoli, S. Meining, E. Meltchakov, R. Mercier, S. Meyer, M. Monecke, F. Monfort, G. Morinaud, F. Moron, L. Mounthey, R. Müller, B. Nicula, S. Parenti, H. Peter, D. Pfiffner, A. Philippon, I. Phillips, J.-Y. Plessier, E. Pyllyser, F. Rabecki, M.-F. Ravet-Krill, J. Rebellato, E. Renotte, L. Rodriguez, S. Roose, J. Rosin, L. Rossi, P. Roth, F. Rouesnel, M. Roulliay, A. Rousseau, K. Ruane, J. Scanlan, P. Schlatter, D.B. Seaton, K. Silliman, S. Smit, P.J. Smith, S.K. Solanki, M. Spescha, A. Spencer, K. Stegen, Y. Stockman, N. Szwec, C. Tamiato, J. Tandy, L. Teriaca, C. Theobald, I. Tychon, L. van Driel-Gesztelyi, C. Verbeeck, J.-C. Vial, S. Werner, M.J. West, D. Westwood, T. Wiegmann, G. Willis, B. Winter, A. Zerr, X. Zhang, A.N. Zhukov, *Astron. Astrophys.* **642**, A8 (2020). <https://doi.org/10.1051/0004-6361/201936663>
- B. Sánchez-Cano, P. Blelly, M. Lester, O. Witasse, M. Cartacci, R. Orosei, H. Opgenoorth, R. Lillis, F. Leblanc, S.E. Milan, P. Conroy, N. Floury, J.M.C. Plane, A. Cicchetti, R. Noschese, A.J. Kopf, *J. Geophys. Res. Space Phys.* **124**, 4556 (2019). <https://doi.org/10.1029/2018ja026403>
- N.M. Schneider, J.I. Deighan, S.K. Jain, A. Stiepen, A.I.F. Stewart, D. Larson, D.L. Mitchell, C. Mazelle, C.O. Lee, R.J. Lillis, J.S. Evans, D. Brain, M.H. Stevens, W.E. McClintock, M.S. Chaffin, M. Crismani, G.M. Holsclaw, F. Lefevre, D.Y. Lo, J.T. Clarke, F. Montmessin, B.M. Jakosky, *Science* **350**, aad0313 (2015). <https://doi.org/10.1126/science.aad0313>
- A. Seppälä, M.A. Clilverd, C.J. Rodger, P.T. Verronen, E. Turunen, *J. Geophys. Res. Space Phys.* **113**, A11311 (2008). <https://doi.org/10.1029/2008ja013517>
- M.D. Smith, *J. Geophys. Res., Planets* **107**, 25 (2002). <https://doi.org/10.1029/2001JE001522>
- M.D. Smith, *Icarus* **167**, 148 (2004). <https://doi.org/10.1016/j.icarus.2003.09.010>
- M.D. Smith, *Icarus* **202**, 444 (2009). <https://doi.org/10.1016/j.icarus.2009.03.027>

- M.D. Smith, J. Geophys. Res., Planets **124**, 2929 (2019). <https://doi.org/10.1029/2019JE006107>
- D.E. Smith, M.T. Zuber, H.V. Frey, J.B. Garvin, J.W. Head, D.O. Muhleman, G.H. Pettengill, R.J. Phillips, S.C. Solomon, H.J. Zwally, W.B. Banerdt, T.C. Duxbury, M.P. Golombek, F.G. Lemoine, G.A. Neumann, D.D. Rowlands, O. Aharonson, P.G. Ford, A.B. Ivanov, C.L. Johnson, P.J. McGovern, J.B. Abshire, R.S. Afzal, X.L. Sun, J. Geophys. Res., Planets **106**, 23689 (2001). <https://doi.org/10.1029/2000je001364>
- M.D. Smith, B.J. Conrath, J.C. Pearl, P.R. Christensen, Icarus **157**, 259 (2002). <https://doi.org/10.1006/icar.2001.6797>
- M.D. Smith, S.W. Bougher, T. Encranaz, F. Forget, A. Kleinböhl, in *The Atmosphere and Climate of Mars*, ed. by R.M. Haberle, R.T. Clancy, F. Forget, M.D. Smith, R.W. Zurek (Cambridge University Press, Cambridge, 2017), pp. 42–75
- M.D. Smith, F. Daerden, L. Neary, A. Khayat, Icarus **301**, 117 (2018). <https://doi.org/10.1016/j.icarus.2017.09.027>
- S.W. Stone, R.V. Yelle, M. Benna, D.Y. Lo, M.K. Elrod, P.R. Mahaffy, Science **370**, 824 (2020). <https://doi.org/10.1126/science.aba5229>
- M.A. Szwest, M.I. Richardson, A.R. Vasavada, J. Geophys. Res., Planets **111**, 5086 (2006). <https://doi.org/10.1029/2005JE002485>
- E.M.B. Thiemann, L. Andersson, R. Lillis, P. Withers, S. Xu, M. Elrod, S. Jain, M.D. Pilinski, D. Pawlowski, P.C. Chamberlin, F.G. Eparvier, M. Benna, C. Fowler, S. Curry, W.K. Peterson, J. Deighan, Geophys. Res. Lett. **45**, 8005 (2018). <https://doi.org/10.1029/2018gl077730>
- T.N. Titus, Mars polar cap edges tracked over 3 full Mars year. Lunar Planet. Sci. Conf. (2005). <https://www.lpi.usra.edu/meetings/lpsc2005/pdf/1993.pdf>. Accessed 30 May 2020
- T.N. Titus, S. Byrne, A. Colaprete, F. Forget, T.I. Michaels, T.H. Prettyman, in *The Atmosphere and Climate of Mars*, ed. by R.M. Haberle, R.T. Clancy, F. Forget, M.D. Smith, R.W. Zurek (Cambridge University Press, Cambridge, 2017), pp. 374–404
- M.G. Trainer, M.H. Wong, T.H. McConnochie, H.B. Franz, S.K. Atreya, P.G. Conrad, F. Lefèvre, P.R. Mahaffy, C.A. Malespin, H.L.K. Manning, J. Martín-Torres, G.M. Martínez, C.P. McKay, R. Navarro-González, Á. Vicente-Retortillo, C.R. Webster, M.-P. Zorzano, J. Geophys. Res., Planets **124**, 3000 (2019). <https://doi.org/10.1029/2019JE006175>
- R.M. Walker, Annu. Rev. Earth Planet. Sci. **3**, 99 (1975). <https://doi.org/10.1146/annurev.ea.03.050175.000531>
- P. Withers, R. Pratt, Icarus **225**, 378 (2013). <https://doi.org/10.1016/j.icarus.2013.02.032>
- M.J. Wolff, M. Lopéz-Valverde, J.-B. Madeleine, R.J. Wilson, M.D. Smith, T. Fouchet, G.T. Delory, in *The Atmosphere and Climate of Mars*, ed. by R.M. Haberle, R.T. Clancy, F. Forget, M.D. Smith, R.W. Zurek (Cambridge University Press, Cambridge, 2017), pp. 106–171
- T.N. Woods, F.G. Eparvier, R. Hock, A.R. Jones, D. Woodraska, D. Judge, L. Didkovsky, J. Lean, J. Mariska, H. Warren, D. McMullin, P. Chamberlin, G. Berthiaume, S. Bailey, T. Fuller-Rowell, J. Sojka, W.K. Tobiska, R. Viereck, Sol. Phys. **275**, 115 (2012). <https://doi.org/10.1007/s11207-009-9487-6>
- S. Xu, E. Thiemann, D. Mitchell, F. Eparvier, D. Pawlowski, M. Benna, L. Andersson, M.W. Liemohn, S. Bougher, C. Mazelle, Geophys. Res. Lett. **45**, 7382 (2018). <https://doi.org/10.1029/2018gl078524>
- R.W. Zurek, Icarus **50**, 288 (1982). [https://doi.org/10.1016/0019-1035\(82\)90127-0](https://doi.org/10.1016/0019-1035(82)90127-0)
- R.W. Zurek, L.J. Martin, J. Geophys. Res., Planets **98**, 3247 (1993). <https://doi.org/10.1029/92je02936>
- R.W. Zurek, R.A. Tolson, S.W. Bougher, R.A. Lugo, D.T. Baird, J.M. Bell, B.M. Jakosky, Ethical statement. J. Geophys. Res. Space Phys. **122**, 3798 (2017). <https://doi.org/10.1002/2016JA023641>

Publisher's Note Springer Nature remains neutral with regard to jurisdictional claims in published maps and institutional affiliations.

Authors and Affiliations

Hessa Almatroushi¹ · Hoor AlMazmi² · Noora AlMheiri¹ · Mariam AlShamsi¹ · Eman AlTunajji¹ · Khalid Badri¹ · Robert J. Lillis³ · Fatma Lootah¹ · Maryam Yousuf¹ · Sarah Amiri¹ · David A. Brain⁴ · Michael Chaffin⁴ · Justin Deighan⁴ · Christopher S. Edwards⁵ · Francois Forget⁶ · Michael D. Smith⁷ · Michael J. Wolff⁸ · Philip R. Christensen⁹ · Scott England¹⁰ · Matthew Fillingim³ · Gregory M. Holsclaw⁴ · Sonal Jain⁴ · Andrew R. Jones⁴ · Mikki Osterloo⁸ · Bruce M. Jakosky⁴ · Janet G. Luhmann³ · Roland M. B. Young¹¹

✉ H. Almatroushi
Hessa.almtroushi@mbrsc.ae

- 1 Mohammed Bin Rashid Space Center, Dubai, UAE
- 2 United Arab Emirates Space Agency, Abu Dhabi, UAE
- 3 Space Sciences Laboratory, University of California Berkeley, Berkeley, CA, USA
- 4 Laboratory for Atmospheric and Space Physics, University of Colorado, Boulder, CO, USA
- 5 Northern Arizona University, Flagstaff, AZ, USA
- 6 Laboratoire de Météorologie Dynamique, Jussieu, Paris, France
- 7 NASA Goddard Space Flight Ctr., Greenbelt, MD, USA
- 8 Space Science Institute, Boulder, CO, USA
- 9 Arizona State University, Tempe, AZ, USA
- 10 Virginia Tech, Blacksburg, VA, USA
- 11 Department of Physics & National Space Science and Technology Center, United Arab Emirates University, Al Ain, UAE